On the degradation of forest ecosystems by extreme events: Statistical Model Checking of a hybrid model

Guillaume Cantin, Benoît Delahaye, Beatriz Funatsu

On the degradation of forest ecosystems by extreme events: Statistical Model Checking of a hybrid model

Guillaume Cantin[1,2], Benoît Delahaye[1], Beatriz M. Funatsu[3]

April 2, 2023

Abstract

In this paper, we study the vulnerability of forest ecosystems perturbed by extreme events, such as those arising from climate change. To investigate the complex interactions between the biological dynamics of the forest and the climatic activity, we construct an original hybrid model, obtained by coupling a continuous reaction-diffusion system, which describes the spatio-temporal dynamics of the forest ecosystem, with a discrete probabilistic process, which models the possible occurrences of extreme events. Properties of ecological interest are considered: invariance of the persistence equilibrium, attraction to the extinction equilibrium and emergence of degraded states. Those properties of the hybrid model are verified through an extension of the Statistical Model Checking framework. We establish the existence of a threshold above which the persistence equilibrium of the forest ecosystem is compromised and give a numerical assessment of this threshold in terms of the probability and intensity of extreme events. We also present non-trivial parameter conditions for which the forest ecosystem converges to a degraded savanna-like state.

Keywords. Hybrid model, model-checking, forest, climate change, reaction-diffusion.

1 Introduction

In the summary for policymakers of its sixth assessment report [39], the Intergovernmental Panel on Climate Change (IPCC) pays particular attention to extreme events arising from climate change, their recent increase in frequency and intensity and their multiple impacts on the equilibrium of both human and natural environments:

> "*Widespread, pervasive impacts to ecosystems, people, settlements, and infrastructure have resulted from observed increases in the frequency and intensity of climate and weather extremes, including hot extremes on land and in the ocean, heavy precipitation events, drought and fire weather. Increasingly since Assessment Report 5, these observed impacts have been attributed to human-induced climate change particularly through increased frequency and severity of extreme events. These include increased heat-related human mortality, warm-water coral bleaching and mortality, and increased drought related tree mortality.*"

Farther in the IPCC report, the cross-chapter dedicated to tropical forests returns in detail on the increased "*tree mortality*" resulting partly from these extreme events:

> "*Climate change is expected to increase temperatures across the tropics, with attendant variability in rainfall, and more extreme events such as intense storms, droughts and wildfires. This could be expected to have structural and functional impacts on tropical forest biomes.*"

[1]Nantes Université, Laboratoire des Sciences du Numérique de Nantes, CNRS, UMR 6004, École Centrale Nantes, F-44000 Nantes, France.
[2]Corresponding author: guillaume.cantin@ls2n.fr
[3]CNRS, UMR 6554 LETG, Bâtiment IGARUN, Campus du Tertre, Nantes Université, France.

Indeed, global tropical forests are double-impacted by the effects of both climate change and human pressures related to land cover changes, such as deforestation, fires, over exploitation, or land management practices [17, 34, 35, 43, 46]. Repeated extreme events such as droughts and floods can have an aggregated, nefarious effect on forest ecosystems by disrupting biogeochemical cycles [13, 41], and increasing their vulnerability to fire spread [6, 45, 47]. Hence, when facing the scientific challenge to better understand the complex dynamics of forest ecosystems, an additional layer of difficulty consists of the overlapping of long-term climate trends (small but steady increase in temperature, for example) and temporally "local" (relative to a long-time frame) events such as recurrent droughts or floods. As extreme events are expected to be more frequent in the context of climate change, the question arises on the capacity of ecosystems to adapt [50], and whether this can lower a tipping point threshold, that is, a change in which a forest ecosystem would irreversibly "tip over", for example, to a savanna-like one [30, 31, 41]. Consequently, a combination of experiments, observations and process-based models is necessary to improve our understanding of forest resilience and tipping points under both global climate and land cover or land use changes [38, 54]. A great deal of work has already been done in this regard. For instance, the impacts of drought-driven wildfires have been studied for the Central Amazonian forest in [37]; the role of forest ecosystems in the fluxes of carbon have been analyzed in [5], [11] or [51]; hydrological services of the forests are investigated in [9] or in [10]; interactions with wildlife and biodiversity are studied in [33]; original models coupling the dynamics of trees and grass have also been analyzed in [4], [15], [24] or in [42], and it has been proved that their spatial structure well reproduces ecologically relevant patterns. Finally, the dynamics of transition from forest to savanna have been investigated for instance in [18], [28], [49]. Numerous other relevant papers could be here cited as well. Nevertheless, challenges still remain to be taken up, both on the observational constraints of tipping point indicators as well as constraints regarding the intrinsic stochastic nature of the forest ecosystem.

In this paper, we aim at contributing to this understanding by modeling the vulnerability of forest ecosystems to extreme events arising from climate change, using an innovative hybrid model that combines deterministic and probabilistic components for trajectory projections of tipping points. Indeed, the deterministic part of the hybrid model, that we construct for this study, is given by a continuous spatio-temporal model which takes the form of a reaction-diffusion system; this reaction-diffusion system, firstly presented in [25], reproduces the biological dynamics of the forest in absence of extreme events. Several properties of this continuous forest model have been already analyzed in [26], [7], [8] and [22]; in particular, the existence of non trivial stationary solutions, which take the form of discontinuous patterns, and their interpretation as the formation of ecotones have been well described; a non-spatial version of this model which takes into account the unpredictability resulting from environmental, ecological and biological disturbances has also been studied in [48]. However, the continuous reaction-diffusion model is incapable of reproducing the impacts of extreme events on the dynamics of the forest, hence needs to be significantly improved. To remedy this lack, our choice is to couple the initial deterministic reaction-diffusion system with a discrete probabilistic process, so as to take into account the possible occurrences of localized extreme events. In this probabilistic process, the times at which extreme events occur, as well as their geographical position, are the results of discrete random variables; moreover, the frequency and the intensity of extreme events are integrated in the model as free parameters, which allows us to test several quantitative scenarios of increase of such events. In this way, our hybrid model is obtained by coupling two spatial scales – *regional* scale for the biological dynamics of the forest ecosystem and *local* scale for the occurrence of an extreme event –, and two modeling formalisms – continuous-deterministic formalism for the forest dynamics and discrete-probabilistic formalism for extreme events. To the best of our knowledge, such a multi-scale and multi-formalism parametric model has never been considered for studying the complex interactions between the biological dynamics of a forest ecosystem and climatic perturbations. The design of this hybrid model represents the first significant contribution of our work. With this innovative hybrid model in hand, we are in position to investigate how extreme events arising from climate change affect the equilibrium and health of forest ecosystems, as highlighted in the IPCC assessment report cited above. The questions we ask mainly concern the stability of the forest-climate ecosystem: *How and to*

what extent can extreme events destabilize the biological persistence of a forest? Is there a threshold, in terms of frequency and intensity of the extreme events, above which this persistence is compromised? If the persistence of the forest is lost, what kind of emergent dynamics can be expected?

To investigate these ecological questions, we choose to apply an extension of the *Statistical Model Checking* framework. This computational approach, which was originally designed for the formal analysis of engineering and industrial systems [20, 27, 53], has very recently encountered a new success in the study of complex systems arising in life sciences, as in [23, 29, 32, 40] notably. Based on the possibility of producing a great number of simulations of probabilistic models, this technique yields statistical guarantees on the analysis of properties of the model under study. Applying this Statistical Model Checking method on our hybrid model, we will establish two important patterns. First, we will show that the forest-climate hybrid model clearly exhibits the existence of a tipping point, over which the persistence equilibrium of the forest can be suddenly broken. By *suddenly*, it should be understood that a very small increase in the frequency or the intensity of extreme events can be fatal to the equilibrium of the forest. Secondly, and this is the main contribution of our work, it turns out that overcoming this tipping-point leads to emergent dynamics of degraded forest, quite far from a forest extinction state. We emphasize that these degraded forest dynamics cannot be described by a single deterministic model, and thus appear as the result of the antagonism between the deterministic and the probabilistic processes which constitute our hybrid model. On this point, our statements corroborate the results obtained with other approaches in the aforementioned papers [4], [18] and [28]. Therefore, the degradation pattern of the forest-climate ecosystem is described through an innovative and explanatory approach.

This paper is organized as follows. In Section 2, the design of our hybrid model is presented in detail and its well-posedness is established at a theoretical level. In Section 3, we present the main features of the Statistic Model Checking method and its adaptation to the forest-climate hybrid model; we also formulate several properties of ecological interest to be verified by the Statistic Model Checking engine, in order to analyze the dynamics of the forest-climate ecosystem. In Section 4, we expose the results of our computational procedure and partly answer the questions addressed above on the dynamics of the forest-climate ecosystem. The proofs of our theoretical results, although abstract, provide a solid framework to our Statistical Model Checking procedure, which relies on the possibility of performing a great number of faithful numerical simulations of the model. Since they involve a technical mathematical background, they are given in the Appendix. Finally, we end our paper with a conclusion in which we summarize our results and give perspectives for further work.

2 Construction of a continuous-deterministic and discrete--probabilistic hybrid model

In this section, our aim is to construct an innovative hybrid model in order to describe the perturbation of a forest ecosystem by extreme events arising from climate change. The dynamics of the forest ecosystem, in absence of perturbations, are modeled by a continuous and deterministic reaction-diffusion system. We then integrate the effects of extreme events by coupling the initial model with a discrete and probabilistic process.

2.1 Spatio-temporal model describing the dynamics of the forest ecosystem in absence of climatic perturbations

Consider a geographical region occupied by a forest ecosystem. We intend to describe the dynamics of this forest ecosystem by a continuous and deterministic model. To that aim, we choose to consider a spatio-temporal model determined by an aged-structured system of three reaction-diffusion equations; this reaction-diffusion system has been first presented in [25], as a forest kinematics model able to

reproduce the formation of ecotones. It is given by the following equations:

$$\begin{cases} \dfrac{\partial u}{\partial t}(t,x) = \beta\delta w(t,x) - \gamma\big(v(t,x)\big)u(t,x) - fu(t,x), & t>0, \quad x\in\Omega, \\ \dfrac{\partial v}{\partial t}(t,x) = fu(t,x) - hv(t,x), & t>0, \quad x\in\Omega, \\ \dfrac{\partial w}{\partial t}(t,x) = d\Delta w(t,x) - \beta w(t,x) + \alpha v(t,x), & t>0, \quad x\in\Omega. \end{cases} \tag{1}$$

Here, the domain $\Omega \subset \mathbb{R}^2$ models the geographical region occupied by the forest ecosystem (a *domain* of $\mathbb{R}^2$ is an open and connected subset of $\mathbb{R}^2$). The unknowns $u = u(t,x)$, $v = v(t,x)$, $w = w(t,x)$ are functions of the time variable $t \in \mathbb{R}^+$ (expressed in years) and of the space variable $x = (x_1, x_2) \in \Omega$, which denote respectively the densities of young trees, old trees and seeds. The parameters α, β, δ, d, f, h are positive coefficients; α and β correspond respectively to the seeds production by old trees and seeds deposition rates; δ models the establishment rate of seeds; d is the diffusion constant of seeds; f is the aging rate of young trees and h is the mortality rate of old trees. The function γ determines the mortality rate of young trees and is chosen so as to admit a minimum for a certain optimal value of v; it is defined by $\gamma(v) = a(v-b)^2 + c$, with positive coefficients a, b, c. The units of each parameter are given in Table 1.

Table 1: Unknowns and parameters of the reaction-diffusion system (1).

Unknown	Symbol	Unit
Young trees density	$u(t,\,x)$	$\text{trees} \times \text{ha}^{-1}$
Old trees density	$v(t,\,x)$	$\text{trees} \times \text{ha}^{-1}$
Seeds density	$w(t,\,x)$	$\text{seeds} \times \text{ha}^{-1}$
Parameter	**Symbol**	**Unit**
Seeds production rate	α	yr^{-1}
Seeds deposition rate	β	yr^{-1}
Seeds establishment rate	δ	yr^{-1}
Aging rate of young trees	f	yr^{-1}
Parameters of competition	a	$\text{trees}^{-2} \times \text{ha}^2 \times \text{yr}^{-1}$
between young and old trees	b	$\text{trees} \times \text{ha}^{-1}$
	c	yr^{-1}
Diffusion rate of seeds	d	$\text{ha}^2 \times \text{yr}^{-1}$
Mortality rate of old trees	h	yr^{-1}

Next, the reaction-diffusion system (1) is supplemented with a boundary condition of Neumann type, which can be written

$$\frac{\partial w}{\partial \nu}(t,x) = 0, \tag{2}$$

on $(0,+\infty) \times \partial\Omega$, where $\partial\Omega$ denotes the boundary of Ω, ν the normal outward vector to $\partial\Omega$. The Neumann boundary condition (2), which guarantees the well-posedness of the mathematical model, means that seeds can accumulate at the boundary of the domain Ω partly occupied by the forest ecosystem, but cannot cross it; this condition is satisfied if the forest domain is bordered by oceans for instance.

Finally, initial conditions are defined at $t = 0$ by

$$u(0,x) = u_0(x), \qquad v(0,x) = v_0(x), \qquad w(0,x) = w_0(x), \qquad x \in \Omega. \tag{3}$$

It is worth noting that the diffusion operator Δ applies only to the seeds density w, since the densities u and v describe the evolution of trees, which are biological individuals obviously not subject to spatial

displacements. For that reason, system (1) is usually called a *partly* dissipative reaction-diffusion system. The existence and uniqueness of non negative and bounded solutions to that system have been proved in [26], where the existence and stability of homogeneous steady states have also been investigated.

We now briefly describe the stability of the homogeneous steady states of the forest model (1), as established in [26]. In the parameter regime given by

$$h > \frac{f\alpha\delta}{c+f}, \tag{4}$$

which corresponds to a large value of the mortality rate of old trees h, with respect to other parameters, system (1) admits a unique homogeneous and stable steady state $O = (0, 0, 0)$, which corresponds to the extinction of the forest ecosystem.

System (1) undergoes a first bifurcation when the parameter h decreases and crosses the critical value $\frac{f\alpha\delta}{c+f}$. Indeed, in the parameter regime given by

$$\frac{f\alpha\delta}{ab^2+c+f} < h < \frac{f\alpha\delta}{c+f}, \tag{5}$$

system (1) admits a second homogeneous and stable steady state P^+ given by

$$P^+ = \left(\frac{h}{f}\left(b+\sqrt{D}\right), b+\sqrt{D}, \frac{\alpha}{\beta}\left(b+\sqrt{D}\right)\right), \tag{6}$$

where $D = \frac{f\alpha\delta - h(c+f)}{ah}$. The stable steady state P^+ given by (6) corresponds to the persistence of the forest ecosystem; P^+ and O are separated by an unstable steady state P^- given by

$$P^- = \left(\frac{h}{f}\left(b-\sqrt{D}\right), b-\sqrt{D}, \frac{\alpha}{\beta}\left(b-\sqrt{D}\right)\right).$$

Afterwards, system (1) undergoes a second bifurcation when the parameter h decreases further and crosses the second critical value $\frac{f\alpha\delta}{ab^2+c+f}$. Therefore, in the parameter regime given by

$$h < \frac{f\alpha\delta}{ab^2+c+f}, \tag{7}$$

which corresponds to a low mortality rate of old trees, system (1) admits only two homogeneous and steady states points: the unstable steady state P^- vanishes, the extinction steady state O becomes unstable, while the persistence steady state P^+ given by (6) remains stable.

From the ecological point of view, the situation corresponding to the parameter regime (7), with a low mortality rate h, is the most favorable: the resulting instability of the extinction steady state O means that the forest ecosystem can recover its persistence state P^+, even if starting from a very low density of trees. On the contrary, the parameter regime (4), with a large mortality rate h, describes the worst situation: even if starting from a large density of trees, the forest ecosystem can be attracted to the extinction equilibrium O. Finally, the parameter regime (5) can be viewed as a transition regime, which is characterized by uncertain dynamics. Among those transition dynamics, various degraded forms of the forest are possible, in particular its transformation into a savanna-like ecosystem.

One remarkable property of the reaction-diffusion system is that it also admits an infinite number of heterogeneous steady states, as proved in [26], which take the form of discontinuous patterns. The stability of these discontinuous patterns seems difficult to study; partial results have however been obtained in [22]. We will show in this work that the discontinuous patterns can trap the trajectories of the model, once coupled with a discrete probabilistic process modeling extreme events. We show in Figure 1 an example of a spatio-temporal trajectory determined by the reaction-diffusion system (1), with $\alpha = 1$, $\beta = 1$, $\delta = 1$, $f = 1$, $h = 0.35$, $a = 1$, $b = 3$, $c = 1$, $d = 0.1$, in an elliptic domain Ω

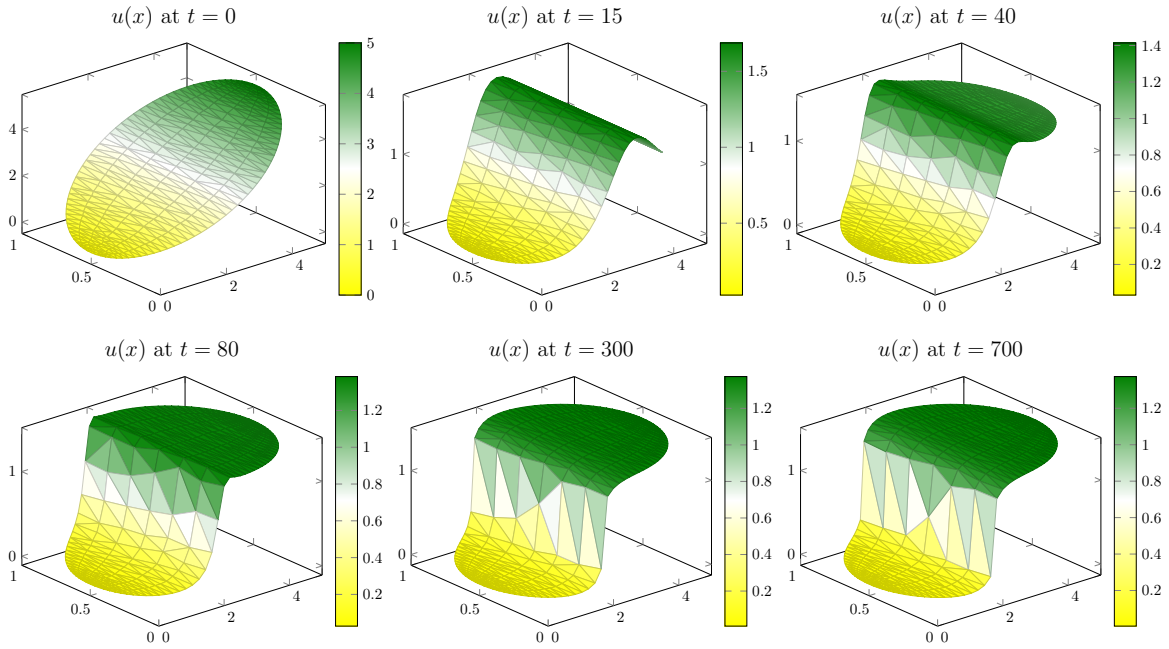

Figure 1: Spatio-temporal trajectory of the reaction-diffusion system (1) reproducing the formation of an ecotone in a forest ecosystem. At $t = 0$, the density $u(x)$ of young trees is distributed over the domain Ω; when t increases ($t = 15, 40, 80, 30, 700$), $u(x)$ converges to a positive value on a subset of Ω (green part of the surface), and to 0 on its complement (yellow part of the surface). The ecotone is located at the frontier between those two subsets.

of dimensions $L = 5$ and $l = 1$; the trajectory was computed with the free and open-source software FreeFem++ [19]. We observe that the model nicely reproduces the formation of ecotones, which are ecological boundaries between the forest and another ecosystem. However, the model is incapable of reproducing the effects of external perturbations such as anthropic activities or extreme events, thus might be improved. It is precisely our aim to integrate the effect of such perturbations in the next section.

2.2 Discrete probabilistic process modeling localized and random extreme events

Now, our aim is to integrate the possible occurrences of extreme events into the reaction-diffusion system (1). Those extreme events can model various perturbations, directly or indirectly linked to climatic conditions such as droughts, fires, or hurricanes, severe floods. They produce a quasi-instantaneous effect on the forest ecosystem, by increasing locally the mortality rate of trees. In order to model the possible occurrences of such extreme events, we introduce three parameters τ, p and I:

- $\tau > 0$ denotes the time delay between two possible occurrences of extreme events;
- $p \in [0, 1]$ denotes the probability of occurrence of a given extreme event at a given time (for simplicity, we assume that p is constant);
- $I \in [0, 1]$ stands for the intensity of the extreme event.

We also introduce a discretization $\mathcal{T}$ of the temporal line $[0, +\infty)$ according to the time step τ:

$$\mathcal{T} = \{0, \tau, 2\tau, \dots, k\tau, \dots\}, \tag{8}$$

and we denote by $\mathcal{E}(t)$ the occurrence of an extreme event at time t. At each time step $k\tau$, $k \in \mathbb{N}^*$, the probability for an extreme event to occur is fixed to p, which can be written

$$\mathbb{P}\big(\mathcal{E}(k\tau)\big) = p, \quad k > 0. \tag{9}$$

If such an event occurs at time $t^\star = k^\star\tau$, then a sub-domain $\omega \subset \Omega$ is chosen randomly as follows: we fix the shape of ω as a disk of constant radius and choose the coordinates of its center uniformly randomly in Ω. Then, the trajectory of the reaction-diffusion system (1) is interrupted and the model restarts according to the dynamics of the reaction-diffusion system (1), with a new initial condition given by

$$\begin{array}{lll} u_0(x) = (1-I)u(t^\star,x), & v_0(x) = (1-I)v(t^\star,x), & \forall x \in \omega, \\ u_0(x) = u(t^\star,x), & v_0(x) = v(t^\star,x), & \forall x \in \Omega \setminus \omega. \end{array} \tag{10}$$

In Equation (10), $u(t,x)$ and $v(t,x)$ denote the two first components of the solution of the reaction-diffusion system (1), defined on $[t^\star - \tau, t^\star)$. The new initial condition models the loss of biological individuals on the localized subdomain ω, with intensity I; for instance, $I = 0.3$ means that 30% of the trees are killed by a localized extreme event on ω. We emphasize that the new initial conditions u_0, v_0 given by (10) are determined by a localized homothetic transformation, which implies that a given extreme event perturbs only a subdomain of the whole forest ecosystem, with a given intensity. Note that the density of seeds $w(t^\star,x)$ is unchanged when an extreme event occurs. Indeed, extreme events can have positive, neutral or negative effects on seeds, depending on the nature of the event, on the trees species or on the type of seeds. For instance, it is observed that fire has no effect on buried seeds, as reported in [44]. The occurrence of such a localized extreme event is schematized in Figure 2. For two distinct occurrences of extreme events at times $t^\star$ and $\tilde{t}^\star$, the corresponding subdomains ω and $\tilde{\omega}$ are *a priori* distinct.

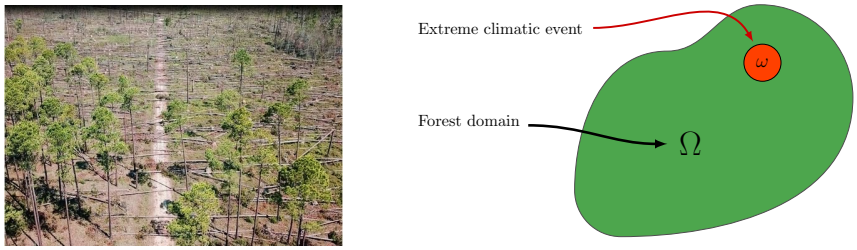

Figure 2: Impact of extreme events on forest ecosystems. Left: Localized forest loss after Hurricane Laura (2020) in Louisiana, USA (source: U.S. Department of Agriculture Forest Service). Right: Schematic illustration of an extreme event occurring in a subdomain ω of a forest domain Ω. Such extreme events occur with a given probability p and yield the loss of trees on the localized subdomain ω, with a given intensity I.

Overall, equations (1)–(2)–(3)–(9)–(10) determine a hybrid continuous/discrete and deterministic/probabilistic model; for convenience the hybrid model is denoted $(\mathcal{H})$; in other words, we have:

$$(\mathcal{H}) \Leftrightarrow (1) - (2) - (3) - (9) - (10). \tag{11}$$

The hybrid model $(\mathcal{H})$ is constructed as a sequence of temporal events, in which the continuous-deterministic dynamics of the forest model (1) and the discrete-probabilistic dynamics of the extreme events (9) alternate successively. This hybrid model is expected to reproduce the perturbations of the forest ecosystem by extreme events arising from climate change, as schematized in Figure 3.

The main question we are interested in is to determine how the stability of the persistence steady state P^+ given in (6) can be altered by the possible occurrences of extreme events. In particular, we wonder if, for a fixed intensity I, a probability threshold $\hat{p}$ exists, above which the persistence equilibrium is destabilized (or if, for a fixed probability p, an intensity threshold $\hat{I}$ exists, causing a

similar effect). In other words, we aim to study the level of vulnerability of the forest ecosystem under the effect of an increase of extreme events.

So as to provide a solid theoretical framework for the analysis of its properties, we have established the well-posedness of the hybrid model ($\mathcal{H}$) given by (11). Indeed, our computational procedure needs to perform a high number of numerical simulations of the hybrid model ($\mathcal{H}$). The relevance of this type of approach can only be justified by a theoretical result proving that the numerical simulations we perform are a fair and confident reflection of the model. Otherwise, the results that follow would lose their fundament. Since it involves a technical mathematical background, the proof is given in the Appendix.

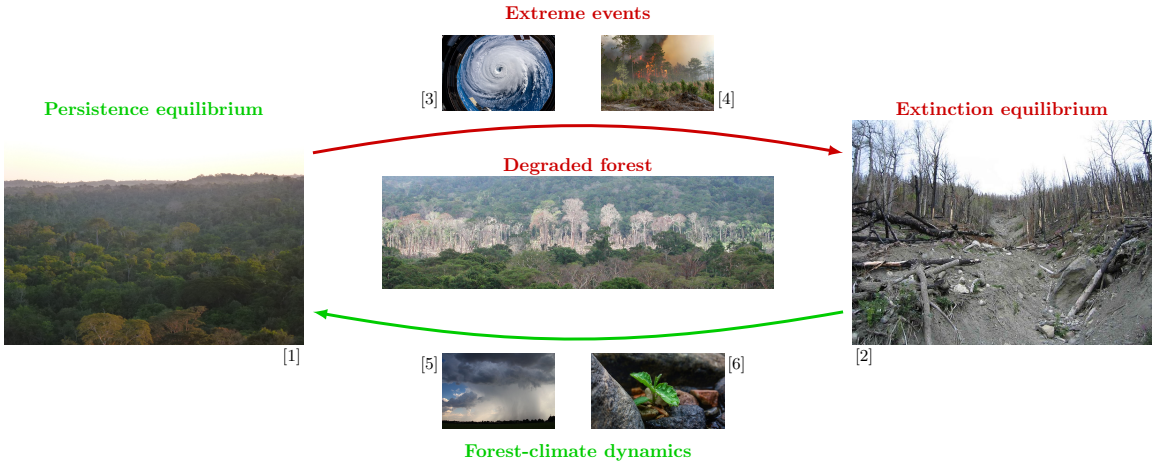

Figure 3: Schema illustrating the hybrid model ($\mathcal{H}$) given by (11), describing the dynamics of the forest ecosystem perturbed by extreme events. In absence of extreme events, the persistence equilibrium is stable and can be recovered thanks to the effect of forest-climate dynamics, even when starting from a low density of trees in a degraded forest state. Under the effect of extreme events, the persistence equilibrium can be destabilized and the forest can be attracted to an extinction state or at least to a degraded state (Sources of the pictures: [1] Beatriz M. Funatsu; [2-6] Wikimedia Commons; [7] NASA/JPL-Caltech).

3 Statistical Model Checking of the hybrid model

In this section, we propose to explore its dynamics with a computational approach. As mentioned previously, the most important question we are interested in is to determine how and to what extent the occurrences of extreme events can destabilize the persistence equilibrium of the forest ecosystem. Since the hybrid model is constructed by coupling a continuous-deterministic formalism with a discrete-probabilistic one, classical techniques from the theory of differential equations do not apply. To overcome this issue, we propose an innovative method, where we handle the study of the dynamics of the hybrid model ($\mathcal{H}$) with a Statistical Model Checking approach (SMC).

SMC relies on the possibility to perform a great number of simulations of the model under study. We therefore start by describing how to compute numerical simulations of the hybrid model ($\mathcal{H}$) and how the set of simulations of ($\mathcal{H}$) constitutes a measurable set.

3.1 Numerical simulations of the hybrid model

We here provide a complete description of the numerical treatment of the hybrid model ($\mathcal{H}$). First, we fix the values of each parameter, except for the probability p for an extreme event to occur and for its intensity I (see Table 2), which we allow to vary in the interval $[0, 1]$. We emphasize that the

parameters values are mostly taken from [1], where the non-spatial forest model, which serves as a basis for the spatialized model (1), has been calibrated. Note also that the values of the parameters lead to the parameter regime (7), in which the continuous dynamics are characterized by the coexistence of the persistence stable steady state P^+ and the extinction unstable steady state O. All numerical computations were performed on the calculation servers of the LS2N (Laboratoire des Sciences du Numérique de Nantes, France), in a GNU/LINUX environment, using the free and open-source software FreeFem++ [19] (the source code of our numerical computations is provided along with this paper as supplementary material). The occurrences of extreme events were simulated by a sequence of independent Bernoulli variables $(Y_k)_{k\geq 0}$ of parameter p. The shape and size of the localized subdomains $(\omega_k)_{k\geq 0}$ where the extreme events occur were fixed to a disk of constant radius, but the coordinates of their centers were randomly generated with a sequence of independent uniform distributions $(Z_k)_{k\geq 0}$ over Ω.

Table 2: Numerical values of the parameters of the hybrid model $(\mathcal{H})$ given by (11).

Deterministic parameters	Value
α	0.5
β	0.5
δ	0.268
f	0.017
a	0.006
b	0.247
c	0.01
d	50
h	0.04

Time variable	
t	$[0, 1000]$
Probabilistic parameters	**Value**
p	$\{0.1, 0.2, \ldots, 0.9\}$
τ	1
I	$\{0.1, 0.2, \ldots, 0.9\}$
Domain parameters	
Ω	Disk of radius 25
ω	Disk of radius 3

For each pair $(p, I) \in \{0.1, 0.2, \ldots, 0.9\}^2$, we have performed two samples of $N = 1200$ numerical simulations of the hybrid model $(\mathcal{H})$, for a total of $2 \times 81 \times 1200 = 194400$ simulations. As will be detailed below, this number of simulations provides statistical guarantees on the formal analysis of the properties of the hybrid model $(\mathcal{H})$. Since the time needed for each simulation was approximately 8 minutes, we have parallelized the computations by constituting 9 groups of 18 parallel simulations of 1200 successive trajectories. Overall, the calculations were spread over about 3 months.

For each simulation, the initial condition U_0 was fixed and defined as a small perturbation of the persistence steady state $P^+ = (u^+, v^+, w^+)$, given by

$$u_0(x) = u^+ + \varepsilon(x), \quad v_0(x) = v^+ + \varepsilon(x), \quad w_0(x) = w^+ + \varepsilon(x),$$

with $\varepsilon(x) > 0$, where $x = (x_1, x_2)$ denotes the space variable in Ω.

3.2 Analysis and visualization of the trajectories

Each trajectory corresponds to a solution $\mathbb{U}(t)$ of the hybrid model $(\mathcal{H})$, which can be visualized in several ways. The complete visualization of a trajectory requires us to produce an animation of the surfaces determined by the densities $u(x)$, $v(x)$ and $w(x)$ over the time interval of the simulation[4]. However, these complete visualizations do not provide a suitable material for analyzing the properties of the hybrid model. Instead, we choose to visualize a projection of the trajectories on a three dimensional environment, by computing, for each value of the time variable t, two indicators of a given trajectory. Those indicators are determined by the distances $d\big(P^+, \mathbb{U}(t)\big)$ and $d\big(O, \mathbb{U}(t)\big)$ of the current point $\mathbb{U}(t)$ of the trajectory to the persistence steady state P^+ and to the extinction steady state O respectively.

[4]Spatio-temporal animations of the hybrid forest-climate model $(\mathcal{H})$ are provided through the following link: https://pagesperso.ls2n.fr/~cantin-g/forestclimate.html.

This projection determines a mapping

$$\begin{array}{rcl} \Theta & \longrightarrow & \mathbb{R}^3 \\ \mathbb{U}(t) & \longmapsto & \pi(t) = \Big(t, d\big(P^+, \mathbb{U}(t)\big), d\big(O, \mathbb{U}(t)\big)\Big), \end{array} \tag{12}$$

where Θ is the phase space of the hybrid model, given by (22). We borrow the vocabulary of the Model Checking framework by saying that $\pi(t)$ is the *trace* corresponding to the trajectory $\mathbb{U}(t)$.

For verifying the properties of the hybrid model $(\mathcal{H})$, we need to follow the position of the trace $\pi(t)$ in $\mathbb{R}^3$, so as to express, for instance, if it is far from the persistence steady state P^+ or not. To that aim, we consider the neighborhoods $\Sigma_\eta(P^+)$ and $\Sigma_{\eta'}(O)$ of P^+ and O respectively, defined for $\eta > 0$ and $\eta' > 0$ by

$$\begin{aligned} \Sigma_\eta(P^+) &= \{\xi \in (\mathbb{R}^+)^3 \mid d(P^+, \xi) < \eta \times d(P^+, O)\}, \\ \Sigma_{\eta'}(O) &= \{\xi \in (\mathbb{R}^+)^3 \mid d(O, \xi) < \eta' \times d(P^+, O)\}, \end{aligned} \tag{13}$$

where d is the standard Euclidean distance in $\mathbb{R}^3$. For instance, $\Sigma_{0.15}(P^+)$ contains all the points $\xi \in (\mathbb{R}^+)^3$ whose distance to P^+ is less than 15% of the distance from P^+ to O.

Overall, the three dimensional environment of the traces $\pi(t)$ of the hybrid model $(\mathcal{H})$ is presented in Figure 4. The horizontal axis on the left depicts the time variable t; the horizontal axis on the front shows the distance $d\big(P^+, \mathbb{U}(t)\big)$ between the trajectory $\mathbb{U}(t)$ and the persistence steady state P^+; the vertical axis on the left shows the distance $d\big(O, \mathbb{U}(t)\big)$ between the trajectory $\mathbb{U}(t)$ and the extinction steady state O. Since the persistence equilibrium P^+ is constant over time and is far from the extinction equilibrium O, it is represented by the green line (top left of the box); the subset $\Sigma_\eta(P^+)$ around P^+ determines a region where the trace $\pi(t)$ remains in a neighborhood of P^+. Similarly, the extinction equilibrium O is far from P^+ and it is represented by the red line (bottom right of the box); the subset $\Sigma_{\eta'}(O)$ determines a neighborhood of the extinction equilibrium. The subsets $\Sigma_\eta(P^+)$ and $\Sigma_{\eta'}(O)$ are separated by an uncertain region of great interest, which we denote $\Gamma(\eta, \eta')$ and which can be defined as the complement of $\Sigma_\eta(P^+) \cup \Sigma_{\eta'}(O)$ in $(\mathbb{R}^+)^3$. Equivalently, $\Gamma(\eta, \eta')$ can be written

$$\Gamma(\eta, \eta') = \big\{\xi \in (\mathbb{R}^+)^3 \mid d\big(P^+, \xi\big) \geq \eta \times d(P^+, O), d\big(O, \xi\big) \geq \eta' \times d(P^+, O)\big\}. \tag{14}$$

Note that the uncertain region $\Gamma(\eta, \eta')$ is likely to attract the trajectories of the hybrid model $(\mathcal{H})$.

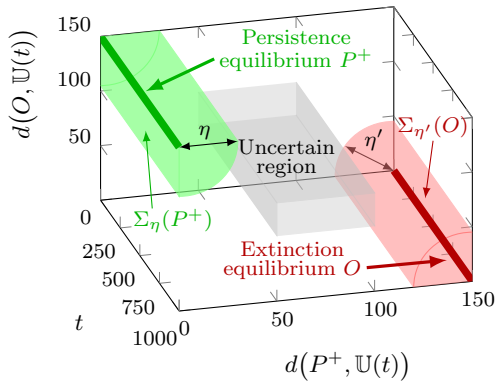

Figure 4: Three dimensional environment for the visualization of a trace $\pi(t)$ of the hybrid model $(\mathcal{H})$. The horizontal axis on the left depicts the time variable t; the horizontal axis on the front shows the distance $d\big(P^+, \mathbb{U}(t)\big)$ between the trajectory $\mathbb{U}(t)$ and the persistence state P^+; the vertical axis on the left shows the distance $d\big(O, \mathbb{U}(t)\big)$ between the trajectory $\mathbb{U}(t)$ and the extinction state O.

As an example, several traces of the hybrid model $(\mathcal{H})$ are shown in Figure 5. The legend depicts the values of the parameters p (probability for an extreme event to occur) and I (intensity of an

extreme event). Those traces exhibit a discontinuous shape which is characteristic from probabilistic processes. Some of the traces remain in the neighborhood $\Sigma_\eta(P^+)$ of the persistence steady state P^+ (top left of the box), whereas other traces are attracted in the neighborhood $\Sigma_{\eta'}(O)$ of the extinction equilibrium O. In between, other traces are attracted in the uncertain region $\Gamma(\eta, \eta')$.

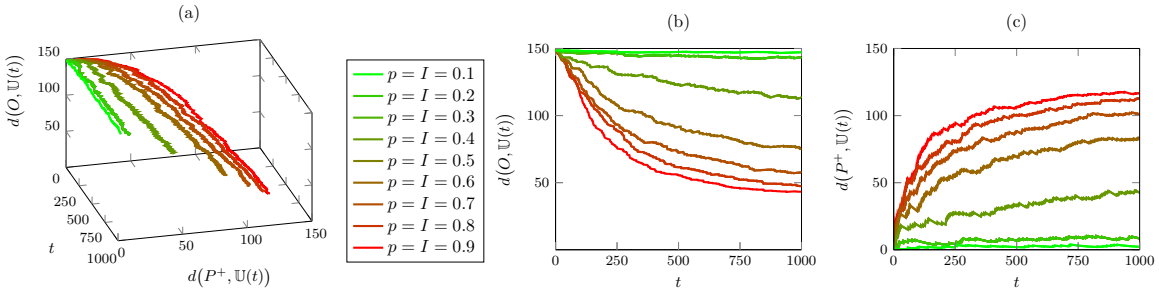

Figure 5: Several traces of the forest-climate hybrid model ($\mathcal{H}$) for different values of the parameters p (probability for an extreme event to occur) and I (intensity of an extreme event). The traces can be visualized (a) in a three dimensional environment: for a low value of p and I, the trace remains in a neighborhood of the persistence equilibrium P^+; for a large value of p and I, it is attracted in a neighborhood of the extinction equilibrium O; in between, other traces are attracted in the uncertain region $\Gamma(\eta, \eta')$. The traces can be projected (b) in the plane $\big(t, d\big(O, \mathbb{U}(t)\big)\big)$; or (c) in the plane $\big(t, d\big(P^+, \mathbb{U}(t)\big)\big)$.

Finally, we consider the whole set of traces of the hybrid model ($\mathcal{H}$), given by

$$\mathsf{Traces} = \Big\{\pi : [0,\infty) \to \mathbb{R}^3 \mid \exists\, \mathbb{U}(t) \text{ solution of } (\mathcal{H}), \pi(t) = \big(t, d(P^+, \mathbb{U}(t)), d(O, \mathbb{U}(t))\big)\Big\}. \tag{15}$$

3.3 Computational procedure of the Statistical Model Checking engine

In this section, we introduce the technique we use to evaluate our model. This procedure is based on the Statistical Model Checking (SMC) technique [27], a technique whose aim is to estimate the probability that a given model satisfies a given property. This technique has been first developed in the context of computer science models, but has recently been used in the context of life sciences, with a special emphasis on models determined by Ordinary Differential Equations [23, 29, 32, 40]. In essence, the model is equipped with a probability measure on its set of traces, and the aim of SMC is to estimate the measure of the subset of traces that satisfies the property of interest. In order to perform this estimation, SMC relies on extensive sampling of the model traces and statistic techniques – in our case the Monte-Carlo method – to compute an estimation of the measure of the subset of traces of interest with formal guarantees regarding the precision and error rate of this estimation.

Let $\Phi \subseteq \mathsf{Traces}$ be the subset of traces of interest. In practice, we use a formula to describe this subset (see Section 3.4 below), and identify it with the property of interest. Given a trace $\pi \in \mathsf{Traces}$, we write $\pi \models \Phi$ and say that π satisfies Φ whenever we have $\pi \in \Phi$.

Let $\varepsilon > 0$ be a precision factor and $\mu \in (0,1)$ be an error rate. In order to perform the estimation using the Monte-Carlo method, we sample a fixed amount $(\pi_i)_{1\leq i\leq N}$ of traces of the hybrid model ($\mathcal{H}$). Each trace π_i is associated with a Boolean random variable X_i regarding the satisfaction of Φ, i.e. $X_i = 1$ if and only if $\pi_i \models \Phi$. Informally, because the random variables $(X_i)_{1\leq i\leq N}$ are independent and identically distributed, the Central Limit theorem [36] states that the limit of $\frac{1}{N}\sum_{1\leq i\leq N} X_i$ when $N \to \infty$ is a good estimation of the measure of Φ. Formally, using Theorem 1 in [20], we obtain the following result as soon as $N \geq 4\log\left(\frac{2}{\mu}\right)/\varepsilon^2$:

$$\mathbb{P}\left(\left|\mathbb{P}(\Phi) - \frac{1}{N}\sum_{1\leq i\leq N} X_i\right| \leq \varepsilon\right) \geq 1-\mu. \tag{16}$$

This technique therefore allows us to compute the number of samples required to obtain a given precision and error rate when performing our estimation. In the following, we will consider precision and error rate parameters of $\varepsilon = \mu = 0.1$, which will therefore require $N \geq 1200$ samples of our model for each property of interest.

3.4 Properties of the hybrid model of ecological interest

In absence of extreme events, we have explained that the forest model (1) is characterized, for the parameter regime (7), by the coexistence of the stable persistence equilibrium P^+ and the unstable extinction equilibrium O. For those who aim to preserve the natural equilibrium of the forest ecosystem, it is a major challenge to maintain the stability of the persistence state. Hence, it is natural to wonder if the occurrences of extreme events can destabilize the persistence equilibrium P^+. If P^+ is destabilized, then we wish to characterize the new behavior of the forest-climate ecosystem: *Is the ecosystem attracted to the extinction equilibrium? Is there a threshold over which the extinction equilibrium becomes attractive? Is the ecosystem able to resist the attraction of the extinction equilibrium? Can it exhibit emergent properties, such as the convergence to a new equilibrium? How could such a new equilibrium be interpreted?* A myriad of similar questions of great interest could be formulated. Here, we choose to focus on the four following properties for a given trace $\pi(t)$ on the hybrid model $(\mathcal{H})$.

- **Property 1: invariance of a neighborhood of the persistence equilibrium P^+.** This property is parametrized by $\eta > 0$ and it is written $\Phi_1(\eta)$; it can be formulated as follows:

$$\Phi_1(\eta) \equiv \forall t \in \mathcal{T}, \pi(t) \in \Sigma_\eta(P^+),$$

  where $\mathcal{T}$ denotes the discretization of the time interval given by (8). Property $\Phi_1(\eta)$ means that the trace $\pi(t)$ remains near the persistence equilibrium during the whole time interval $\mathcal{T}$.

- **Property 2: attraction to a neighborhood of the extinction equilibrium O.** This second property is parametrized by $\eta' > 0$. Two variants $\Phi_2(\eta')$ and $\Psi_2(\eta')$ can be considered.

  – Temporary attraction : $\Phi_2(\eta') \equiv \exists\, \hat{t} \in \mathcal{T}$ such that $\pi(\hat{t}) \in \Sigma_{\eta'}(O)$.

  – Definitive attraction : $\Psi_2(\eta') \equiv \exists\, \hat{t} \in \mathcal{T}$ such that $\forall t > \hat{t}, \pi(t) \in \Sigma_{\eta'}(O)$.

  Property $\Phi_2(\eta')$ means that the trace $\pi(t)$ eventually enters $\Sigma_{\eta'}(O)$, and might or not remain in $\Sigma_{\eta'}(O)$; property $\Psi_2(\eta')$ means that the trace enters and remains in $\Sigma_{\eta'}(O)$. Obviously, $\Psi_2(\eta')$ implies $\Phi_2(\eta')$; however, we will prove that the traces which satisfy $\Phi_2(\eta')$ but not $\Psi_2(\eta')$ are rare.

- **Property 3: oscillations between a neighborhood of the persistence equilibrium P^+ and a neighborhood of the extinction equilibrium O.** This property is parametrized by $\eta > 0$, $\eta' > 0$; it is written $\Phi_3(\eta, \eta')$ and can be formulated as follows:

$$\Phi_3(\eta, \eta') \equiv \exists\, (t_n)_{n \geq 0} \subset \mathcal{T} \text{ such that } \begin{array}{l} t_n < t_{n+1}, \forall n \geq 0, \\ \pi(t_{2k}) \in \Sigma_\eta(P^+), \\ \pi(t_{2k+1}) \in \Sigma_{\eta'}(O), \forall k \geq 0. \end{array}$$

  Although we can prove the existence of traces which satisfy $\Phi_3(\eta, \eta')$, it will turn out that such traces are very rare.

- **Property 4: attraction to the uncertain region $\Gamma(\eta, \eta')$.** This property is also parametrized by $\eta > 0$, $\eta' > 0$; as for property 2, two variants $\Phi_4(\eta, \eta')$ and $\Psi_4(\eta, \eta')$ can be formulated as follows.

  – Temporary attraction : $\Phi_4(\eta, \eta') \equiv \exists\, \hat{t} \in \mathcal{T}$ such that $\pi(\hat{t}) \in \Gamma(\eta, \eta')$.

  – Definitive attraction : $\Psi_4(\eta, \eta') \equiv \exists\, \hat{t} \in \mathcal{T}$ such that $\forall t > \hat{t}, \pi(t) \in \Gamma(\eta, \eta')$.

From the ecological point of view, property $\Phi_1(\eta)$ is the most important to satisfy, since it ensures that the forest ecosystem remains in a neighborhood of the persistence equilibrium P^+; the smaller η, the more the persistence equilibrium P^+ is preserved. At the opposite, properties $\Phi_2(\eta')$ or $\Psi_2(\eta')$ should be avoided, since they mean that the forest ecosystem converges to an extinction state. It could happen that the forest ecosystem is temporarily attracted to the extinction equilibrium O, but recovers the persistence equilibrium P^+ after a certain time; this situation is expressed by the oscillation property $\Phi_3(\eta, \eta')$. Finally, properties $\Phi_4(\eta, \eta')$ or $\Psi_4(\eta, \eta')$ specify that the forest-climate ecosystem reaches an intermediate equilibrium, far from both the persistence equilibrium and the extinction equilibrium; as mentioned previously, savanna-like ecosystems or degraded forests can correspond to such intermediate equilibria.

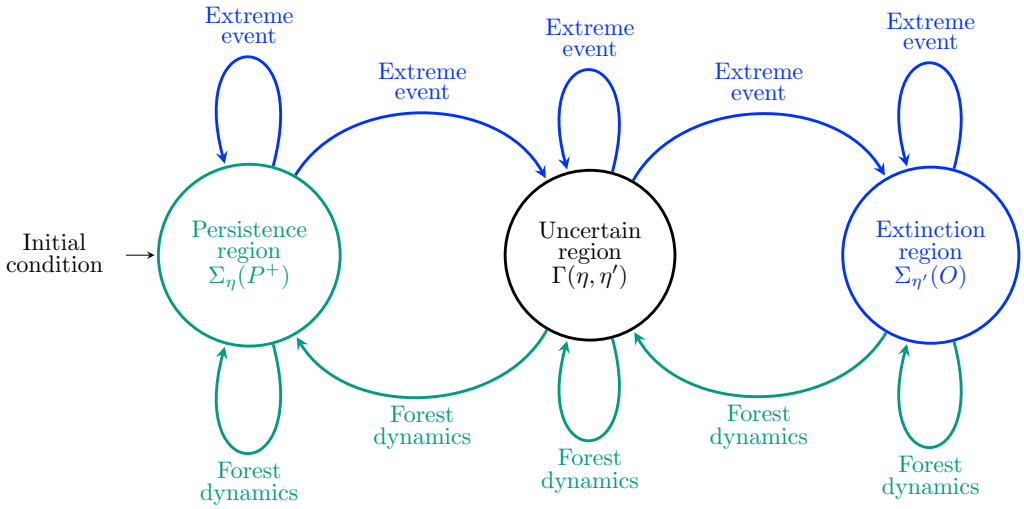

Figure 6: Schematic representation illustrating the hybrid model ($\mathcal{H}$), with three states $\Sigma_\eta(P^+)$, $\Sigma_{\eta'}(O)$, $\Gamma(\eta, \eta')$. Biological dynamics and extreme events induce antagonist transitions between those states.

4 Results of the Statistical Model Checking analysis and discussion

In this final section, we present and discuss the results of the formal analysis on the properties $\Phi_1(\eta)$, $\Phi_2(\eta')$, $\Psi_2(\eta')$, $\Phi_3(\eta, \eta')$, $\Phi_4(\eta, \eta')$ and $\Psi_4(\eta, \eta')$ specified above. Our results are given as confidence intervals of the form (16), on the probability for each property to be satisfied by the hybrid model($\mathcal{H}$) given by (11). However, in order to present our results in a clear manner, we adopt the following notations:

$$\begin{aligned} \mathbb{P}(\phi) \simeq \xi \quad &\Leftrightarrow \quad \mathbb{P}\big(\mathbb{P}(\phi) \in [\xi - \varepsilon, \xi + \varepsilon]\big) \geq 1 - \mu, \\ \mathbb{P}(\phi) \gtrsim \xi \quad &\Leftrightarrow \quad \mathbb{P}\big(\mathbb{P}(\phi) \geq \xi - \varepsilon\big) \geq 1 - \mu, \end{aligned}$$

for a given property ϕ and $\xi \in [0, 1]$, with $\varepsilon = \mu = 10\%$.

Since the properties to be verified depend on the parameters p (probability for an extreme event to occur) and I (intensity of an extreme event), we provide several color maps where we depict the probability of each property with respect to p and I.

4.1 Invariance of the persistence equilibrium and existence of a tipping point

We begin with the results for the probability of property $\Phi_1(\eta)$, which describes the invariance of the persistence equilibrium P^+. We show in Figure 7 four color maps for the estimation of the probability $\mathbb{P}\big(\Phi_1(\eta)\big)$, with respect to the parameters p (probability for an extreme event to occur), I (intensity of an extreme event), and for $\eta \in \{0.1, 0.2, 0.3, 0.4\}$, which measures the size of the neighborhood $\Sigma_\eta(P^+)$. As an example, by virtue of the first color map (top left in Figure 7), we have $\mathbb{P}\big(\Phi_1(0.1)\big) \simeq 1$ for $p = I = 0.1$ and $\mathbb{P}\big(\Phi_1(0.1)\big) \simeq 0$ for $p = I = 0.9$. More generally, we observe that for each value of $\eta \in \{0.1, 0.2, 0.3, 0.4\}$, the color map is divided into two zones; the green zone corresponds to the values of p and I for which we have $\mathbb{P}\big(\Phi_1(\eta)\big) \simeq 1$, whereas the blue zone corresponds to the values of p and I for which we have $\mathbb{P}\big(\Phi_1(\eta)\big) \simeq 0$. The following proposition gathers our numerical results.

Proposition 1. *For each $\eta \in \{0.1, 0.2, 0.3, 0.4\}$, the parameter domain $D = \{0.1, 0.2, \ldots, 0.9\}^2$ of (p, I) admits two subdomains $G_1(\eta)$, $B_1(\eta)$ satisfying:*

$$\begin{aligned}
&G_1(\eta) \neq \varnothing, \quad B_1(\eta) \neq \varnothing, \quad G_1(\eta) \cap B_1(\eta) = \varnothing,\\
&\mathbb{P}\big(\Phi_1(\eta)\big) \simeq 1 \text{ if } (p, I) \in G_1(\eta),\\
&G_1(0.1) \subset G_1(0.2) \subset G_1(0.3) \subset G_1(0.4),\\
&\mathbb{P}\big(\Phi_1(\eta)\big) \simeq 0 \text{ if } (p, I) \in B_1(\eta),\\
&B_1(0.1) \supset B_1(0.2) \supset B_1(0.3) \supset B_1(0.4).
\end{aligned} \tag{17}$$

Proposition 1 can be interpreted as follows: for p and I sufficiently small, the trajectory of the hybrid model $(\mathcal{H})$ remains in a neighborhood of the persistence equilibrium P^+ (with a probability near from 1); in other words, the forest ecosystem is *not* destabilized by extreme events if they are rare and of low intensity. At the opposite, if p and I increase, then the trajectory of the hybrid model $(\mathcal{H})$ leaves the neighborhood of the persistence equilibrium P^+; hence, the forest ecosystem is altered by frequent extreme events of strong intensity. Moreover, the larger the size η of the neighborhood $\Sigma_\eta(P^+)$, the larger the green zone, the smaller the blue zone.

We also observe that the transition between the green zone and the blue zone is abrupt, which implies that the forest ecosystem can be very sensitive to a small increase of extreme events. This abrupt transition corresponds to a *tipping point*, where the dynamics of the forest ecosystems are profoundly modified. It can be visualized in a different manner in Figure 8, which has been obtained for $\eta = 0.3$ by sectioning the color map for $\Phi_1(0.3)$ along the line of equation $p = I$. It is worth noting that this tipping point is a *bifurcational* tipping point, since it emerges under the variation of one parameter of the model. However, this bifurcational tipping point also presents similarities with *noise-induced* tipping points [3], since it is the result of the coupling of a continuous process with a probabilistic one.

Remark 1 (Existence of a tipping point)**.** *We emphasize that the existence of a tipping point is established in a parametric abstract framework, which, although not finely calibrated to any given forest ecosystem, necessarily covers the "real-world" parameters values, which shall be determined in a separate work for the Amazon basin.*

4.2 Temporary or definitive attraction to the extinction equilibrium

We continue with the results for the probabilities of the properties $\Phi_2(\eta')$ and $\Psi_2(\eta')$, which describe respectively a temporary attraction and a definitive attraction to the extinction equilibrium O. These properties are parametrized by $\eta' > 0$, which measures the size of the neighborhood $\Sigma_{\eta'}(O)$, and also depend on p and I.

We present in Figure 9 four color maps for $\eta' \in \{0.3, 0.35, 0.4, 0.45\}$, showing estimations of the probabilities of the temporary attraction property $\Phi_2(\eta')$. On these color maps, the green zones

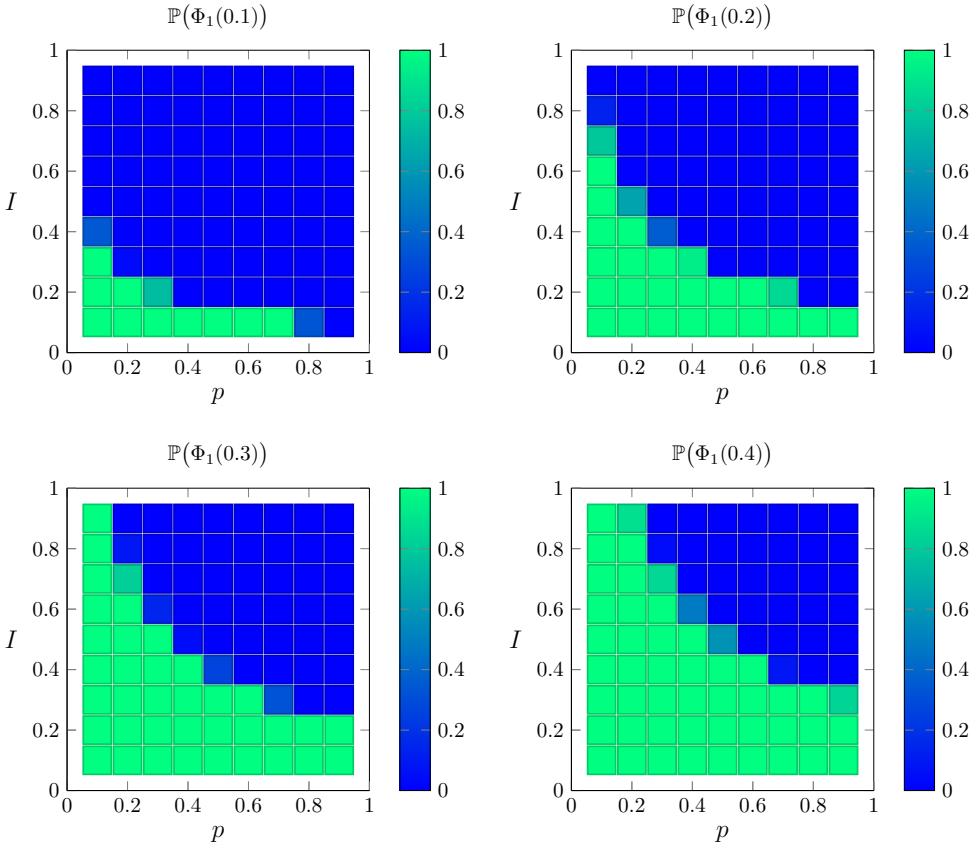

Figure 7: Estimation of the probability of property $\Phi_1(\eta)$ (invariance of the persistence equilibrium P^+) with respect to the parameters p (probability for an extreme event to occur) and I (intensity of an extreme event), for $\eta \in \{0.1, 0.2, 0.3, 0.4\}$. If p and I are small enough, then the persistence equilibrium P^+ remains stable. If p and I increase, P^+ looses its stability.

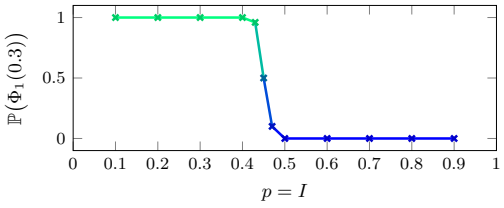

Figure 8: Estimation of the probability of property $\Phi_1(0.3)$ with respect to the parametrization of equation $p = I$, showing an abrupt transition from the green zone where $\Phi_1(0.3) \simeq 1$ to the blue zone where $\Phi_1(0.3) \simeq 0$.

correspond to the values of (p, I) for which $\mathbb{P}\big(\Phi_2(\eta')\big) \simeq 0$, whereas the blue zones correspond to $\mathbb{P}\big(\Phi_2(\eta')\big) \simeq 1$ for $\eta' \in \{0.4, 0.45\}$, $\mathbb{P}\big(\Phi_2(\eta')\big) \gtrsim 0.6$ for $\eta' = 0.3$, $\mathbb{P}\big(\Phi_2(\eta')\big) \gtrsim 0.8$ for $\eta' = 0.35$. Note that we have also computed the probabilities $\mathbb{P}\big(\Phi_2(\eta')\big)$ for $\eta' < 0.3$; in that case, it is observed that $\mathbb{P}\big(\Phi_2(\eta')\big) \simeq 0$ for all (p, I), which leads to a totally green color map. For that reason, we do not depict the results for $\eta' < 0.3$. The following proposition summarizes our numerical results.

Proposition 2. *For each $\eta' < 0.3$ and for all $(p, I) \in \{0.1, 0.2, \ldots, 0.9\}^2$, we have*

$$\mathbb{P}\big(\Phi_2(\eta')\big) \simeq 0. \tag{18}$$

For each $\eta' \in \{0.3, 0.35, 0.4, 0.45\}$, the parameter domain $D = \{0.1, 0.2, \ldots, 0.9\}^2$ of (p, I) admits two subdomains $G_2(\eta')$, $B_2(\eta')$ satisfying:

$$\begin{aligned}
&G_2(\eta') \neq \varnothing, \quad B_2(\eta') \neq \varnothing, \quad G_2(\eta') \cap B_2(\eta') = \varnothing,\\
&\mathbb{P}\big(\Phi_2(0.3)\big) \gtrsim 0.6 \text{ if } (p, I) \in B_2(0.3),\\
&\mathbb{P}\big(\Phi_2(0.35)\big) \gtrsim 0.8 \text{ if } (p, I) \in B_2(0.35),\\
&\mathbb{P}\big(\Phi_2(\eta')\big) \simeq 1 \text{ if } (p, I) \in B_2(\eta'), \eta' \in \{0.4, 0.45\},\\
&B_2(0.3) \subset B_2(0.35) \subset B_2(0.4) \subset B_1(0.45),\\
&\mathbb{P}\big(\Phi_2(\eta')\big) \simeq 0 \text{ if } (p, I) \in G_2(\eta'),\\
&G_2(0.3) \supset G_2(0.35) \supset G_2(0.4) \supset G_2(0.45).
\end{aligned} \tag{19}$$

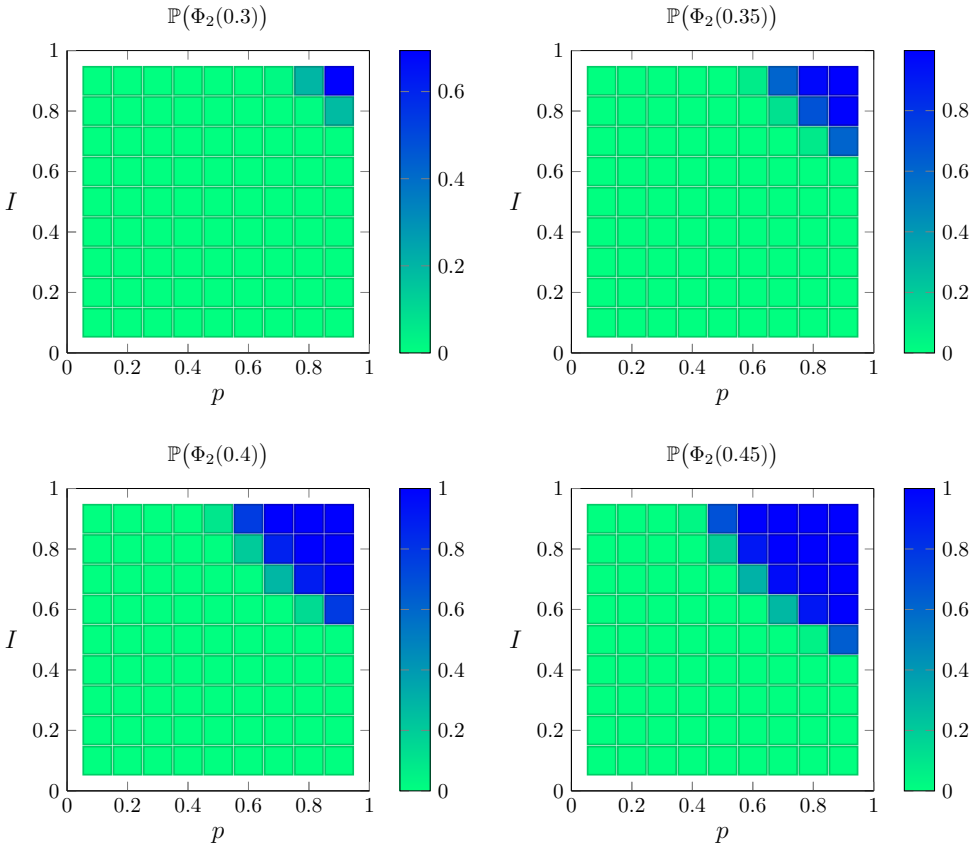

Figure 9: Estimation of the probability of the property $\Phi_2(\eta')$ (temporary attraction to the extinction equilibrium O) with respect to the parameters p (probability for an extreme event to occur) and I (intensity of an extreme event), for $\eta' \in \{0.3, 0.35, 0.4, 0.45\}$. If p and I are small enough, then the extinction equilibrium O is not attractive. If p and I increase, the extinction equilibrium O becomes attractive.

Proposition 2 can also be interpreted with an ecological point of view. First, for large values of p and I, the forest ecosystem is temporarily attracted to a neighborhood $\Sigma_{\eta'}(O)$ of the extinction equilibrium

Table 3: Estimation of the probability $\varrho(\eta', p, I)$ that a trajectory of the hybrid model $(\mathcal{H})$ satisfies the temporary attraction property $\Phi_2(\eta')$ but not the definitive attraction property $\Psi_2(\eta')$, for different values of η', p and I. For other values of η', p and I, this probability is null.

$\eta' = 0.3$			$\eta' = 0.35$			$\eta' = 0.4$			$\eta' = 0.45$		
p	I	$\varrho(\eta', p, I)$	p	I	$\varrho(\eta', p, I)$	p	I	$\varrho(\eta', p, I)$	p	I	$\varrho(\eta', p, I)$
0.7	0.9	1/18	0.6	0.9	3/87	0.5	0.9	9/111	0.4	0.9	6/36
0.8	0.8	1/10	0.7	0.8	6/140	0.6	0.8	18/245	0.5	0.8	25/215
0.8	0.9	3/236	0.7	0.9	17/722	0.6	0.9	29/912	0.5	0.9	23/815
0.9	0.8	12/221	0.8	0.7	8/98	0.7	0.7	24/336	0.6	0.7	40/362
0.9	0.9	7/833	0.8	0.8	16/807	0.7	0.8	11/1039	0.6	0.8	16/1084
			0.8	0.9	8/1159	0.8	0.6	18/166	0.6	0.9	1/1195
			0.9	0.6	1/11	0.8	0.7	8/1063	0.7	0.6	26/332
			0.9	0.7	15/725	0.9	0.6	20/921	0.7	0.7	12/1140
			0.9	0.8	4/1181				0.8	0.5	4/60
									0.8	0.6	18/1091
									0.9	0.5	33/755

O. This means that frequent extreme events of strong intensity, which have already been proved to destabilize the persistence equilibrium P^+, can severely modify the dynamics of the forest ecosystem. Hence, the existence of a tipping point is underpinned (see also Figure 10). However, if the size η' of the neighborhood $\Sigma_{\eta'}(O)$ is small ($\eta' < 0.3$, which is equivalent to $d\big(O, \mathbb{U}(t)\big) < 30\% \times d\big(P^+, O\big)$), then the trajectory of the hybrid model $(\mathcal{H})$ *never* enters $\Sigma_{\eta'}(O)$; in other words, even if the forest ecosystem is attracted towards the extinction equilibrium, it cannot coincide with it, which can be welcomed in a somewhat optimistic manner.

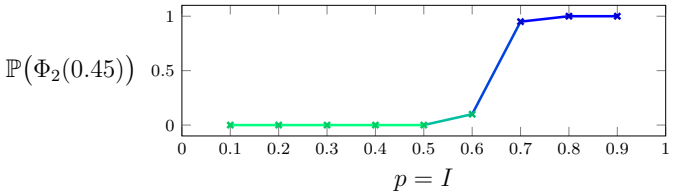

Figure 10: Estimation of the probability of the property $\Phi_2(0.45)$ with respect to the parametrization of equation $p = I$, showing an abrupt transition from the green zone where $\Phi_2(0.45) \simeq 0$ to the blue zone where $\Phi_2(0.45) \simeq 1$.

Let us now discuss on the nature of the attraction towards the extinction equilibrium: *is it always only temporary or may it be definitive?* To answer this question, we have also computed the probabilities of the definitive attraction property $\Psi_2(\eta')$, for the same values of η', p and I. We do not show the corresponding color maps, since they seem to be totally identical. Instead, in order to distinguish the probabilities of $\Phi_2(\eta')$ and $\Psi_2(\eta')$, we have computed an estimation of the probability that a trajectory of the hybrid model $(\mathcal{H})$ satisfies $\Phi_2(\eta')$ but not $\Psi_2(\eta')$. Let us denote by $\varrho(\eta', p, I)$ this estimated probability. For most of the values of η', p and I, it is observed that $\varrho(\eta', p, I)$ is null. The values of η', p and I for which it is positive are shown in Table 3. Over the complete range of η', p and I, the maximum value of $\varrho(\eta', p, I)$ is about 10%.

Those computations show that when the trajectory of the hybrid model $(\mathcal{H})$ is attracted towards the extinction equilibrium O, then, in the great majority of the cases, it remains in a neighborhood of it. In other words, if the dynamics of the forest ecosystem are altered, then the forest ecosystem cannot recover a healthy persistence state, except in rare cases.

4.3 Existence of scarce oscillatory traces and emergence of degraded forest states

Finally, we present the results for the probabilities of property $\Phi_3(\eta, \eta')$, which describes an oscillatory behavior between neighborhoods of the persistence equilibrium P^+ and of the extinction equilibrium O, and of the properties $\Phi_4(\eta, \eta')$, $\Psi_4(\eta, \eta')$ which correspond respectively to a temporary attraction and to a definitive attraction towards the uncertain region $\Gamma(\eta, \eta')$. Those properties are parametrized by $\eta > 0$ and $\eta' > 0$, which measure the sizes of the neighborhoods $\Sigma_\eta(P^+)$ and $\Sigma_{\eta'}(O)$ respectively. Their common point is that they specify non-trivial and emergent dynamics of the forest-climate ecosystem, which cannot be observed in absence of extreme events.

First, we discuss on the existence of oscillatory traces between $\Sigma_\eta(P^+)$ and $\Sigma_{\eta'}(O)$. If η and η' are near from 1, then the neighborhoods $\Sigma_\eta(P^+)$ and $\Sigma_{\eta'}(O)$ can cross, that is $\Sigma_\eta(P^+) \cap \Sigma_{\eta'}(O) \neq \varnothing$; in that case, it is of poor interest to research oscillatory traces between $\Sigma_\eta(P^+)$ and $\Sigma_{\eta'}(O)$. Therefore, the property $\Phi_3(\eta, \eta')$ is relevant only if η and η' are small enough, so that $\Sigma_\eta(P^+)$ and $\Sigma_{\eta'}(O)$ are disjoint. The following theorem establishes the existence of oscillatory traces for the relevant situation. Its proof is given in the Appendix.

Theorem 1. *Assume that the persistence equilibrium P^+ is globally asymptotically stable. Let $\eta > 0$, $\eta' > 0$ be sufficiently small so that $\Sigma_\eta(P^+)$ and $\Sigma_{\eta'}(O)$ are disjoint. Then, for all $p \in (0, 1)$ and all $I \in (0, 1]$, the hybrid model $(\mathcal{H})$ determined by (11) admits traces which satisfy the oscillatory property $\Phi_3(\eta, \eta')$.*

We show in Figure 11 three traces of the hybrid model $(\mathcal{H})$, which satisfy property $\Phi_3(\eta, \eta')$. The existence of oscillatory traces established by Theorem 1 can be viewed as the result of the two antagonist processes which constitute the hybrid model $(\mathcal{H})$: indeed, the continuous-deterministic system (1) reproduces the biological dynamics of the forest ecosystem, which are characterized by the stability of the persistence equilibrium P^+. At the opposite, the discrete-probabilistic process determined by (10) describes the effect of extreme events, which attract the forest ecosystem to the extinction state by increasing the mortality rate of trees.

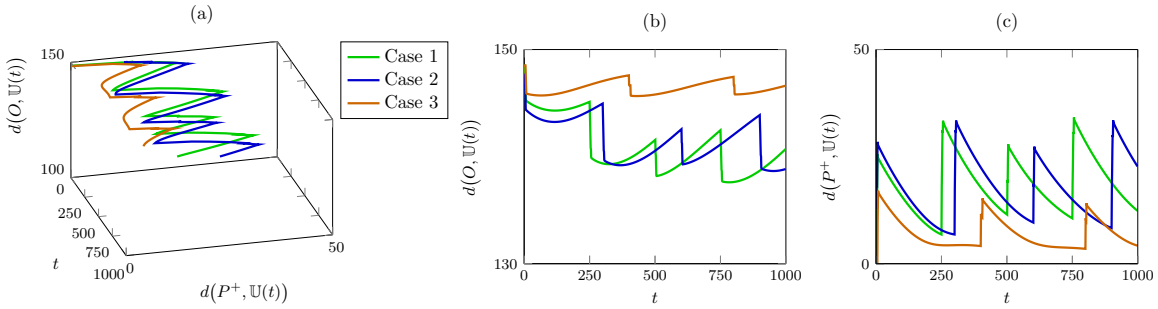

Figure 11: Three traces of the hybrid model $(\mathcal{H})$ which satisfy property $\Phi_3(\eta, \eta')$ of oscillations between a neighborhood $\Sigma_\eta(P^+)$ and a neighborhood $\Sigma_{\eta'}(O)$.

From the ecological point of view, such an oscillatory behavior means that the forest ecosystem can recover the persistence equilibrium P^+ after being attracted to a neighborhood of the extinction equilibrium O. However, we have proved previously that the probability for a trace, which enters a neighborhood of the extinction equilibrium O, to leave this neighborhood is small (see Table 3). Hence, we expect that the probability for a trace to exhibit an oscillatory behavior is even smaller. To verify this paradox, we have computed estimations of the probabilities $\mathbb{P}\big(\Phi_3(\eta, \eta')\big)$ for $(\eta, \eta') \in \{0.1, 0.2, 0.3\}^2$ and $(p, I) \in \{0.1, 0.2, \ldots, 0.9\}^2$, applying again the SMC method. We do not depict the results on color maps, since they are very near from 0 in each case and lead to totally blue color maps. In other words, oscillatory traces theoretically exist, but are practically very rare; indeed, oscillatory traces are

produced by sequences of Bernoulli variables realizations of the form (24), whose probability is very small. We obtain the following proposition.

Proposition 3. *For all* $(\eta, \eta') \in \{0.1, 0.2, 0.3\}^2$ *and for all* $(p, I) \in \{0.1, 0.2, \ldots, 0.9\}^2$*, it holds that* $\mathbb{P}\big(\Phi_3(\eta, \eta')\big) \simeq 0$.

It remains to discuss on the properties $\Phi_4(\eta, \eta')$ and $\Psi_4(\eta, \eta')$, which describe respectively the temporary and definitive attraction towards the uncertain region $\Gamma(\eta, \eta')$ given by (14). Since the definitive attraction is more difficult to satisfy than the temporary attraction, we obviously have $\mathbb{P}\big(\Phi_4(\eta, \eta')\big) \geq \mathbb{P}\big(\Psi_4(\eta, \eta')\big)$ for all $\eta > 0$ and $\eta' > 0$. Here, we focus on the definitive attraction property $\Psi_4(\eta, \eta')$, which models the convergence of the forest ecosystem to a degraded state. We show in Figure 12 four color maps with the estimated probability $\mathbb{P}\big(\Psi_4(\eta, \eta')\big)$, for $\eta = \eta' \in \{0.3, 0.35, 0.4, 0.45\}$ and $(p, I) \in \{0.1, 0.2, \ldots, 0.9\}^2$. In each case, we observe that the parameter domain $D = \{0.1, 0.2, \ldots, 0.9\}^2$ of (p, I) admits two subdomains where $\mathbb{P}\big(\Psi_4(\eta, \eta')\big) \simeq 1$ and $\mathbb{P}\big(\Psi_4(\eta, \eta')\big) \simeq 0$. We summarize our results with the following proposition.

Proposition 4. *For each* $(\eta, \eta') \in \{0.3, 0.35, 0.4, 0.45\}^2$ *such that* $\eta = \eta'$*, the parameter domain* $D = \{0.1, 0.2, \ldots, 0.9\}^2$ *of* (p, I) *admits two subdomains* $G_4(\eta, \eta')$*,* $B_4(\eta, \eta')$ *satisfying:*

$$
\begin{aligned}
&G_4(\eta, \eta') \neq \varnothing, \quad B_4(\eta, \eta') \neq \varnothing, \quad G_4(\eta, \eta') \cap R_4(\eta, \eta') = \varnothing, \\
&\mathbb{P}\big(\Psi_4(\eta, \eta')\big) \simeq 1 \text{ if } (p, I) \in B_4(\eta, \eta'), \\
&B_4(0.3, 0.3) \supset B_4(0.35, 0.35) \supset B_4(0.4, 0.4) \supset B_4(0.45, 0.45), \\
&\mathbb{P}\big(\Psi_4(\eta, \eta')\big) \simeq 0 \text{ if } (p, I) \in G_4(\eta, \eta'), \\
&G_4(0.3, 0.3) \subset G_4(0.35, 0.35) \subset G_4(0.4, 0.4) \subset G_4(0.45, 0.45).
\end{aligned}
\tag{20}
$$

We also observe in Figure 12 that the green subdomain $G_4(\eta, \eta')$ can itself be divided into two subdomains $G_4^{BL}(\eta, \eta')$ (green subdomain at the bottom left of each color map) and $G_4^{TR}(\eta, \eta')$ (green subdomain at the top right of each color map). In $G_4^{BL}(\eta, \eta')$, we have $\mathbb{P}\big(\Psi_4(\eta, \eta')\big) \simeq 0$, which means that the traces of the hybrid model $(\mathcal{H})$ cannot satisfy property $\Psi_4(\eta, \eta')$; in parallel, Proposition 1 shows that in $G_4^{BL}(\eta, \eta')$, we have $\Phi_1(\eta) \simeq 1$. Overall, it means that the traces of the hybrid model $(\mathcal{H})$ remain in a neighborhood of the persistence equilibrium P^+. Similarly, in $G_4^{TR}(\eta, \eta')$, we also have $\mathbb{P}\big(\Psi_4(\eta, \eta')\big) \simeq 0$, but at the same time, by virtue of Proposition 2, we have $\Phi_2(\eta') \simeq 1$, which means that the traces of the hybrid model $(\mathcal{H})$ are attracted to a neighborhood of the extinction equilibrium O. In between, that is, in $B_4(\eta, \eta')$, we have $\mathbb{P}\big(\Psi_4(\eta, \eta')\big) \simeq 1$, which implies that the traces of the hybrid model $(\mathcal{H})$ are definitively attracted to the uncertain region $\Gamma(\eta, \eta')$. Note that the subdomain $B_4(\eta, \eta')$ is determined by intermediate values of p or I, which correspond to extreme events of moderate frequency or moderate intensity.

From the ecological point of view, the uncertain region $\Gamma(\eta, \eta')$ describes intermediate dynamics of the forest-climate ecosystem, far from the persistence equilibrium P^+, but also far from the extinction equilibrium O; low (although positive) densities of trees characterize these intermediate dynamics, which can correspond to savanna-like ecosystems or degraded forest states. In other words, a moderate increase of extreme events is likely to degrade the forest ecosystem and to lead to its savannization.

Remark 2 (Explanatory description of degraded forest ecosystems)**.** *We emphasize that the degradation pattern of the forest is the result of the two antagonist processes which oppose each other in the forest-climate ecosystem: the first process corresponds to the biological dynamics of the forest, whereas the second process corresponds to the occurrences of extreme events. Both processes are integrated in our model with appropriate scales and formalisms: the biological dynamics are modeled with a continuous and deterministic system, whereas the climatic perturbations are modeled by a discrete and probabilistic process. Therefore, our model faithfully reproduces through an explanatory approach the dynamics of forests perturbed by violent climate events.*

It is worth noting that the spatial diffusion of biological constituents of the ecosystem, besides nonlinearity and stochasticity, is a necessary ingredient to reproduce this type of ecological dynamics. On

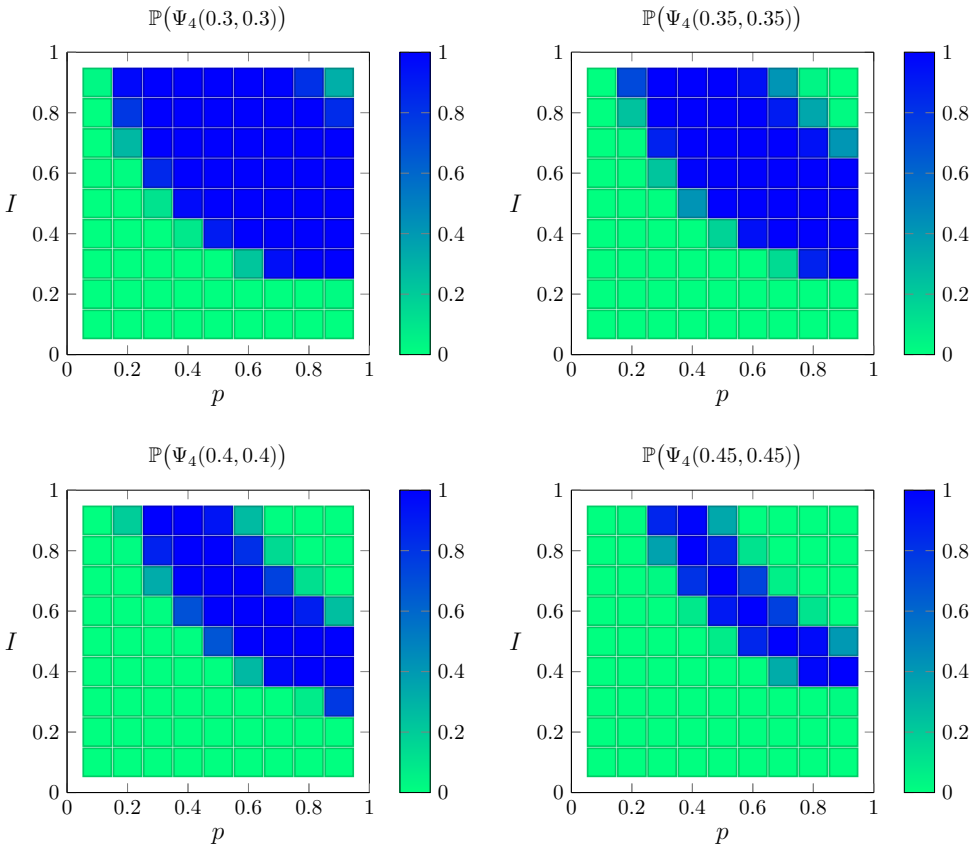

Figure 12: Estimated probability of property $\Psi_4(\eta, \eta')$, which describes the definitive attraction to the uncertain region $\Gamma(\eta, \eta')$, for $\eta = \eta' \in \{0.3, 0.35, 0.4, 0.45\}$ and $(p, I) \in \{0.1, 0.2, \ldots, 0.9\}^2$. This definitive attraction reproduces the degradation of the forest ecosystem.

this point, our results are consistent with the tendencies established in [18], where a different reaction-diffusion model is used to show that dispersal induces spatially aggregated distributions, separated by a stable savanna-forest boundary. The diffusion process has also been identified as a crucial modeling element in [15], where a dryland-vegetation model integrating both seeds dispersal and soil-water diffusion has been considered to analyze the stability and dynamics of desertification fronts.

5 Conclusion and perspectives

In this paper, we have studied the vulnerability of forest ecosystems under the effect of extreme events. We have constructed an innovative hybrid model, by coupling a deterministic and continuous process describing the biological dynamics of the forest, with a discrete and probabilistic process reproducing the occurrences of extreme events. The frequency and the intensity of extreme events are free parameters of the hybrid model, which allows to test several scenarios of increase of such events. The properties of ecological interest of this hybrid parametric model, whose well-posedness has been established at a theoretical level, have been verified by applying the Statistical Model Checking framework. The main patterns highlighted by our computational approach are the following:

- the forest-climate model admits an abrupt tipping-point, in line with observations, over which its persistence is compromised;

- a very small increase of the intensity or of the frequency of extreme events can bring the forest-climate ecosystem to go beyond this tipping-point;
- when the tipping-point is exceeded, the forest-climate can be attracted to an extinction state, but emergent dynamics are observed with a greater probability;
- oscillatory behaviors between extinction and persistence are theoretically possible, but practically very rare;
- the most probable emergent behavior is the convergence towards a degraded savanna-like forest state, far from both the persistence state and the extinction state.

In a near future, we aim to explore two research perspectives. The first perspective concerns the confrontation of our hybrid model to real-world data, so as to provide a fine numerical assessment of the general patterns which we have exhibited in a parametric and abstract framework. As a privileged case study, the Amazon forest is well-known to be particularly vulnerable to both climate and land cover changes [43], with the regions of highest vulnerability in ecosystem function overlapping areas of large-scale forest degradation and fragmentation at the southern and eastern edges of the basin [21, 43]. Recent studies have confirmed that widespread droughts and floods have occurred in the Amazon with increased frequency and intensity in the past two decades, and with changes in precipitation patterns, including extreme precipitation [2, 12, 14, 16, 17, 35, 52]. A combination of the hybrid model and real world data on the forest state (intact versus degraded), land cover (forest or savanna), and extreme events, may thus provide important quantitative insights to the degree of fragility and support the urgency for preservation and protection of the Amazon forest, as a common good of humankind.

Our second research perspective concerns the theoretical study of Model Checking methods for a large class of abstract hybrid models, which would generalize the forest-climate model developed in the present work. In particular, the computational exploration of such hybrid models shall be set in a rigorous probabilistic framework, which implies a thorough discretization of their enormous phase space, as their continuous part can lead to an explosion of the number of their states. Providing a solid theoretical basis to the formal analysis of this type of models, characterized by a multi-scale and multi-formalism structure, will allow to investigate numerous questions similar to the ones studied in this paper, related to the vulnerability of various biological ecosystems perturbed by climate change, not only in forestry, but also in oceanography or glaciology for instance, and more generally to study the great problem of *the stability of the Earth system*.

Acknowledgment

The authors are sincerely grateful to the anonymous reviewers whose comments greatly improved the presentation of the paper.

6 Appendix: Mathematical Background

In this Appendix, we gather the proofs of our main theoretical results, which involve a technical mathematical background.

6.1 Well-posedness of the hybrid model

As the model $(\mathcal{H})$ determined by (11) presents an original hybrid structure, we intend to establish that it admits relevant solutions. Hence, following [26], we introduce the Banach space X defined by

$$X = L^\infty(\Omega) \times L^\infty(\Omega) \times L^2(\Omega), \tag{21}$$

and the subspace $\Theta \subset X$ of non-negative elements of X, given by

$$\Theta = \big\{U = (u,v,w)^\top \in X \mid u \geq 0, v \geq 0, w \geq 0 \text{ on } \Omega\big\}. \tag{22}$$

The occurrences of extreme events at time steps $k\tau \in \mathcal{T}$ ($k \geq 0$) are determined by a sequence of independent Bernoulli variables $(Y_k)_{k\geq 0}$ of constant parameter p. For those $k \geq 0$ such that $Y_k = 1$, the locations $x_k = (x_{1,k}, x_{2,k}) \in \Omega$ of the subdomains ω_k on which the extreme events occur, are determined by a sequence of independent uniform distributions $(Z_k)_{k\geq 0}$ over Ω.

Theorem 2. *For any initial condition $U_0 \in \Theta$, any realization of a sequence of independent Bernoulli variables $(Y_k)_{k\geq 0}$, and any realization of a sequence of independent uniform distributions $(Z_k)_{k\geq 0}$ over Ω, the hybrid model $(\mathcal{H})$ defined by (11) admits a unique global solution $\mathbb{U}(t) = \big(u(t), v(t), w(t)\big)^\top$ defined on $[0, +\infty)$ with values in Θ.*

Furthermore, for each pair (k, k') of positive integers such that $k < k'$, $Y_k = Y_{k'} = 1$ and $Y_j = 0$ for $k < j < k'$, the restriction $\mathbb{U}_{|[k\tau,k'\tau)}$ of $\mathbb{U}$ on the time interval $[k\tau, k'\tau)$ satisfies

$$\begin{aligned} &u_{|[k\tau,k'\tau)}, v_{|[k\tau,k'\tau)} \in \mathscr{C}\big([k\tau, k'\tau), L^\infty(\Omega)\big) \cap \mathscr{C}^1\big((k\tau, k'\tau), L^\infty(\Omega)\big), \\ &w_{|[k\tau,k'\tau)} \in \mathscr{C}\big([k\tau, k'\tau), L^2(\Omega)\big) \cap \mathscr{C}\big((k\tau, k'\tau), H^2_N(\Omega)\big) \cap \mathscr{C}^1\big((k\tau, k'\tau), L^2(\Omega)\big), \end{aligned} \tag{23}$$

where $H^2_N(\Omega) = \{w \in W^{2,2}(\Omega) \mid \frac{\partial w}{\partial \nu} = 0 \text{ on } \partial\Omega\}$.

The function spaces given in (23) mean that on each time interval $[k\tau, k'\tau)$, u, v and w are continuous with respect to the time variable t, but might admit discontinuities with respect to the space variable $x \in \Omega$. Finally, $W^{2,2}(\Omega)$ denotes the usual Sobolev space of functions in $L^2(\Omega)$ admitting first and second derivatives in $L^2(\Omega)$ in the sense of distributions.

Proof. Let us consider an initial condition $U_0 \in \Theta$. As presented in [26], the partly dissipative reaction-diffusion system (1) admits a unique global solution $U(t, U_0) = \big(u(t), v(t), w(t)\big)^\top$ such that

$$\begin{aligned} &u, v \in \mathscr{C}\big([0, \infty), L^\infty(\Omega)\big) \cap \mathscr{C}^1\big((0, \infty), L^\infty(\Omega)\big), \\ &w \in \mathscr{C}\big([0, \infty), L^2(\Omega)\big) \cap \mathscr{C}\big((0, \infty), H_N(\Omega)\big) \cap \mathscr{C}^1\big((0, \infty), L^2(\Omega)\big). \end{aligned}$$

Now, let k_1 denote the first positive integer such that the Bernoulli variable Y_{k_1} satisfies $Y_{k_1} = 1$. The uniform distribution Z_{k_1} determines the location of a subdomain $\omega_{k_1} \subset \Omega$. Therefore, we can construct the solution $\mathbb{U}(t)$ of the hybrid model by setting

$$\begin{aligned} &\mathbb{U}(t) = U(t, U_0), \quad t \in [0, k_1\tau), \\ &\mathbb{U}(k_1\tau) = (u_1, v_1, w_1)^\top, \end{aligned}$$

where u_1, v_1 are given as in (10) by

$$\begin{aligned} &u_1(x) = (1 - I)u(k_1\tau, x), \quad v_1(x) = (1 - I)v(k_1\tau, x), \quad \forall x \in \omega_{k_1}, \\ &u_1(x) = u(k_1\tau, x), \qquad\qquad v_1(x) = v(k_1\tau, x), \qquad\quad \forall x \in \Omega \setminus \omega_{k_1}, \end{aligned}$$

and w_1 is given by $w_1 = w(k_1\tau)$.

Now we consider again the partly dissipative reaction-diffusion system (1) with the new initial condition $U_1 = (u_1, v_1, w_1)^\top$ and the new initial time $t_0 = k_1\tau$; we denote by $\tilde{U}(t, U_1) = \big(\tilde{u}(t), \tilde{v}(t), \tilde{w}(t)\big)$ the resulting global solution on $[k_1\tau, +\infty)$. We introduce the first integer $k_2 > k_1$ such that the Bernoulli variable Y_{k_2} satisfies $Y_{k_2} = 1$, and the uniform distribution Z_{k_2}, which determines the location of a subdomain $\omega_{k_2} \subset \Omega$. The solution $\mathbb{U}(t)$ of the hybrid model is extended to $[0, k_2\tau]$ by setting

$$\begin{aligned} &\mathbb{U}(t) = \tilde{U}(t, U_1), \quad t \in [k_1\tau, k_2\tau), \\ &\mathbb{U}(k_2\tau) = (u_2, v_2, w_2)^\top, \end{aligned}$$

where u_2, v_2 are given by

$$\begin{array}{lll} u_2(x) = (1-I)\tilde{u}(k_2\tau, x), & v_2(x) = (1-I)\tilde{v}(k_2\tau, x), & \forall x \in \omega_{k_2}, \\ u_2(x) = \tilde{u}(k_2\tau, x), & v_2(x) = \tilde{v}(k_2\tau, x), & \forall x \in \Omega \setminus \omega_{k_2}, \end{array}$$

and w_2 is given by $w_2 = \tilde{w}(k_2\tau)$.

Finally, repeating the previous reasoning allows to construct by induction the solution $\mathbb{U}(t)$ of the hybrid model $(\mathcal{H})$ on $[0, \infty)$. The proof is complete. □

Remark 3 (Probability space for the set of traces)**.** *Since each trajectory $\mathbb{U}(t)$ of the hybrid model $(\mathcal{H})$ is the result of a double deterministic-probabilistic process, we can equip the set* Traces *given by (15) with a σ-algebra $\mathscr{F}$ and a probability measure $\mathbb{P}$. Indeed, the occurrences of extreme events given by (9) are fully determined by a sequence of independent Bernoulli variables $(Y_k)_{k\geq 0}$, and the corresponding subdomains $(\omega_k)_{k\geq 0}$ where these extreme events occur are fully determined by a sequence of independent uniform variables $(Z_k)_{k\geq 0}$. Overall, we obtain a probability space $\big(\textsf{Traces}, \mathscr{F}, \mathbb{P}\big)$, where $\mathscr{F}$ is the σ-algebra determined by the sequences $(Y_k)_{k\geq 0}$ and $(Z_k)_{k\geq 0}$ and $\mathbb{P}$ is the associated probability measure.*

6.2 Specification of the properties

Here, we emphasize for the reader interested in Formal Methods that the properties 1 to 4 described in Section 3.4 fully fit with the Model Checking theory framework, since they can be specified by means of the Linear Temporal Logic formalism (LTL). Indeed, the hybrid model $(\mathcal{H})$ admits three states $\Sigma_\eta(P^+)$, $\Sigma_{\eta'}(O)$, $\Gamma(\eta, \eta')$, with both deterministic and probabilistic transitions between those states, as depicted in Figure 6. If the behavior of the hybrid model $(\mathcal{H})$ is observed on the infinite discrete time interval $\mathcal{T} = \{0, 1, 2, \dots\}$, we can write:

$$\begin{aligned} \Phi_1(\eta) &\equiv \Box\Sigma_\eta(P^+), \\ \Phi_2(\eta') &\equiv \Diamond\Sigma_{\eta'}(O), \\ \Psi_2(\eta') &\equiv \Diamond\Box\Sigma_{\eta'}(O), \\ \Phi_3(\eta, \eta') &\equiv \Box\big(\Sigma_\eta(O) \Rightarrow \Diamond\Sigma_{\eta'}(P^+)\big) \wedge \Box\big(\Sigma_{\eta'}(P^+) \Rightarrow \Diamond\Sigma_\eta(O)\big), \\ \Phi_4(\eta, \eta') &\equiv \Diamond\big(\neg\Sigma_\eta(O) \wedge \neg\Sigma_{\eta'}(P^+)\big), \\ \Psi_4(\eta, \eta') &\equiv \Diamond\Box\big(\neg\Sigma_\eta(O) \wedge \neg\Sigma_{\eta'}(P^+)\big), \end{aligned}$$

where $\Diamond$ and $\Box$ denote the temporal operators *eventually* and *always* respectively, $\wedge$ denotes the conjunction connector and $\neg$ the negation operator. If the behavior of the hybrid model $(\mathcal{H})$ is observed on a finite time interval $\mathcal{T} = \{0, 1, 2, \dots, T\}$ with T a positive integer, then one should replace $\Diamond$ by $\Diamond^{\leq T}$ and $\Box$ by $\Box^{\leq T}$ in the specification of the properties.

6.3 Existence of oscillatory traces: proof of Theorem 1

Let us denote by $\mathbb{U}(t)$ the solution of the hybrid model $(\mathcal{H})$ and by $(X_k)_{k\geq 0}$ the sequence of Bernoulli variables which determine if an extreme event $\mathcal{E}(k\tau)$ occurs at $t = k\tau$. We consider a particular sequence of realizations $(X_k)_{k\geq 0}$ satisfying

$$\begin{cases} X_k = 1, & k_1 \times j \leq k < k_1 \times j + k_2, \\ X_k = 0, & k_1 \times j + k_2 \leq k < k_1 \times (j+1), \end{cases} \tag{24}$$

for all $j \geq 0$, where k_1, k_2 are positive integers such that $k_1 > k_2$. With such a sequence $(X_k)_{k\geq 0}$, the solution $\mathbb{U}(t)$ undergoes k_2 successive extreme events $\mathcal{E}(k\tau)$, which alternate with a time interval of length $(k_1 - k_2)\tau$ without any extreme event.

If k_2 is sufficiently large, then the solution $\mathbb{U}(t)$ is attracted to a neighborhood $\Sigma_{\eta'}(O)$ of the extinction equilibrium O on the time interval $[k_1 j\tau, (k_1 j + k_2)\tau]$, for all $j \geq 0$. Next, since P^+ is globally asymptotically stable, if k_1 if sufficiently large, then the solution $\mathbb{U}(t)$ comes back in a neighborhood $\Sigma_\eta(P^+)$ on the time interval $[(k_1 j + k_2)\tau, k_1(j+1)\tau]$, for all $j \geq 0$.

Therefore, the solution $\mathbb{U}(t)$ oscillates between $\Sigma_\eta(P^+)$ and $\Sigma_{\eta'}(O)$. The proof is complete.

References

[1] M. Y. Antonovsky, R. Fleming, Y. A. Kuznetsov, and W. Clark. Forest-pest interaction dynamics: The simplest mathematical models. *Theoretical Population Biology*, 37(2):343–367, 1990.

[2] D. Arvor, B. M. . Funatsu, V. Michot, and V. Dubreuil. Monitoring rainfall patterns in the Southern Amazon with PERSIANN-CDR data: Long-term characteristics and trends. *Remote Sensing*, 9:889, 2017.

[3] P. Ashwin, S. Wieczorek, R. Vitolo, and P. Cox. Tipping points in open systems: bifurcation, noise-induced and rate-dependent examples in the climate system. *Philosophical Transactions of the Royal Society A: Mathematical, Physical and Engineering Sciences*, 370(1962):1166–1184, 2012.

[4] J. Banasiak, Y. Dumont, and I. V. Yatat Djeumen. Spreading speeds and traveling waves for monotone systems of impulsive reaction–diffusion equations: application to tree–grass interactions in fire-prone savannas. *Differential Equations and Dynamical Systems*, pages 1–34, 2020.

[5] R. Betts, M. Sanderson, and S. Woodward. Effects of large-scale Amazon forest degradation on climate and air quality through fluxes of carbon dioxide, water, energy, mineral dust and isoprene. *Philosophical Transactions of the Royal Society B: Biological Sciences*, 363(1498):1873–1880, 2008.

[6] P. M. Brando, B. Soares-Filho, L. Rodrigues, A. Assunção, D. Morton, D. Tuchschneider, E. C. M. Fernandes, M. N. Macedo, U. Oliveira, and M. T. Coe. The gathering firestorm in southern amazonia. *Science Advances*, 6(2):eaay1632, 2020.

[7] G. Cantin. Non-existence of the global attractor for a partly dissipative reaction-diffusion system with hysteresis. *Journal of Differential Equations*, 299:333–361, 2021.

[8] G. Cantin, A. Ducrot, and B. M. Funatsu. Mathematical modeling of forest ecosystems by a reaction–diffusion–advection system: impacts of climate change and deforestation. *Journal of Mathematical Biology*, 83(6):1–45, 2021.

[9] G. Cantin and N. Verdière. Networks of forest ecosystems: Mathematical modeling of their biotic pump mechanism and resilience to certain patch deforestation. *Ecological Complexity*, 43:100850, 2020.

[10] C. Carvalho-Santos, J. P. Honrado, and L. Hein. Hydrological services and the role of forests: Conceptualization and indicator-based analysis with an illustration at a regional scale. *Ecological Complexity*, 20:69–80, 2014.

[11] Z. Dai, K. Johnson, R. Birdsey, J. Hernandez-Stefanoni, and J. Dupuy. Assessing the effect of climate change on carbon sequestration in a mexican dry forest in the yucatan peninsula. *Ecological complexity*, 24:46–56, 2015.

[12] N. S. Debortoli, V. Dubreuil, B. Funatsu, F. Delahaye, C. H. de Oliveira, S. Rodrigues-Filho, C. H. Saito, and R. Fetter. Rainfall patterns in the Southern Amazon: a chronological perspective (1971–2010). *Climatic Change*, 132:251–264, 2015.

[13] D. Ellison, C. E. Morris, B. Locatelli, D. Sheil, J. Cohen, D. Murdiyarso, V. Gutierrez, M. van Noordwijk, I. F. Creed, J. Pokorny, D. Gaveau, D. V. Spracklen, A. B. Tobella, U. Ilstedt, A. J. Teuling, S. G. Gebrehiwot, D. C. Sands, B. Muys, B. Verbist, E. Springgay, Y. Sugandi, and C. A. Sullivan. Trees, forests and water: Cool insights for a hot world. *Global Environmental Change*, 43:51–61, 2017.

[14] J. C. Espinoza, J. Ronchail, J. A. Marengo, and H. Segura. Contrasting north-south changes in Amazon wet-day and dry-day frequency and related atmospheric features (1981-2017). *Climate Dyn.*, 52:5413–5430, 2019a.

[15] C. Fernandez-Oto, O. Tzuk, and E. Meron. Front instabilities can reverse desertification. *Physical review letters*, 122(4):048101, 2019.

[16] R. Fu, L. Yin, W. Li, P. A. Arias, R. E. Dickinson, L. Huang, S. Chakraborty, K. Fernandes, B. Liebmann, R. Fisher, and R. B. Myneni. Increased dry-season length over southern Amazonia in recent decades and its implication for future climate projections. *Proc. Natl. Acad. Sci. (USA)*, 110(45):18110–18115, 2013.

[17] B. M. Funatsu, R. Le Roux, D. Arvor, J. C. Espinoza, C. Claud, J. Ronchail, V. Michot, and V. Dubreuil. Assessing precipitation extremes (1981–2018) and deep convective activity (2002–2018) in the Amazon region with CHIRPS and AMSU data. *Climate Dyn.*, pages 1–23, 2021.

[18] N. Goel, V. Guttal, S. A. Levin, and A. C. Staver. Dispersal increases the resilience of tropical savanna and forest distributions. *The American Naturalist*, 195(5):833–850, 2020.

[19] F. Hecht. New development in FreeFem++. *Journal of numerical mathematics*, 20(3-4):251–266, 2012.

[20] T. Hérault, R. Lassaigne, F. Magniette, and S. Peyronnet. Approximate probabilistic model checking. In *International Workshop on Verification, Model Checking, and Abstract Interpretation*, pages 73–84. Springer, 2004.

[21] M. Hirota, M. Holmgren, E. H. Van Nes, and M. Scheffer. Global resilience of tropical forest and savanna to critical transitions. *Science*, 334(6053):232–235, 2011.

[22] S. Iwasaki. Asymptotic convergence of solutions to the forest kinematic model. *Nonlinear Analysis: Real World Applications*, 62:103382, 2021.

[23] D. Julien, G. Cantin, and B. Delahaye. End-to-end statistical model checking for parametric ODE models. *To be published in the Proceedings of QEST Conference*, 2022.

[24] P. Klimasara and M. Tyran-Kamińska. A model for random fire induced tree-grass coexistence in savannas. *Mathematica Applicanda*, 46(1), 2018.

[25] Y. A. Kuznetsov, M. Y. Antonovsky, V. Biktashev, and E. Aponina. A cross-diffusion model of forest boundary dynamics. *Journal of Mathematical Biology*, 32(3):219–232, 1994.

[26] C. Le Huy, T. Tsujikawa, and A. Yagi. Stationary solutions to forest kinematic model. *Glasgow Mathematical Journal*, 51(1):1–17, 2009.

[27] A. Legay, B. Delahaye, and S. Bensalem. Statistical model checking: An overview. In *International conference on runtime verification*, pages 122–135. Springer, 2010.

[28] Q. Li, A. C. Staver, S. A. Levin, et al. Spatial feedbacks and the dynamics of savanna and forest. *Theoretical Ecology*, 12(2):237–262, 2019.

[29] B. Liu, B. M. Gyori, and P. Thiagarajan. Statistical model checking-based analysis of biological networks. In *Automated Reasoning for Systems Biology and Medicine*, pages 63–92. Springer, 2019.

[30] T. E. Lovejoy and C. Nobre. Amazon tipping point. *Science Advances*, 4(2):eaat2340, 2018.

[31] T. E. Lovejoy and C. Nobre. Amazon tipping point: Last chance for action. *Science Advances*, 5(12):eaba2949, 2019.

[32] T. Mancini, E. Tronci, I. Salvo, F. Mari, A. Massini, and I. Melatti. Computing biological model parameters by parallel statistical model checking. In *International Conference on Bioinformatics and Biomedical Engineering*, pages 542–554. Springer, 2015.

[33] F. Mora. A suite of ecological indicators for evaluating the integrity of structural eco-complexity in Mexican forests. *Ecological Complexity*, 50:101001, 2022.

[34] C. A. Nobre, G. Sampaio, L. S. Borma, J. C. Castilla-Rubio, J. S. Silva, and M. Cardoso. Land-use and climate change risks in the Amazon and the need of a novel sustainable development paradigm. *Proc. Natl. Acad. Sci. (USA)*, 113(39):10759–10768, 2016.

[35] J. S. Panisset, R. Libonati, C. M. P. Gouveia, F. Machado-Silva, D. A. França, J. R. A. França, and L. F. Peres. Contrasting patterns of the extreme drought episodes of 2005, 2010 and 2015 in the Amazon Basin. *International Journal of Climatology*, 38(2):1096–1104, 2018.

[36] V. V. Petrov. *Sums of Independent Random Variables*. De Gruyter, 2022.

[37] A. Pontes-Lopes, C. V. Silva, J. Barlow, L. M. Rincón, W. A. Campanharo, C. A. Nunes, C. T. de Almeida, C. H. Silva Júnior, H. L. Cassol, R. Dalagnol, et al. Drought-driven wildfire impacts on structure and dynamics in a wet Central Amazonian forest. *Proceedings of the Royal Society B*, 288(1951):20210094, 2021.

[38] R. Portela and I. Rademacher. A dynamic model of patterns of deforestation and their effect on the ability of the Brazilian Amazonia to provide ecosystem services. *Ecological Modelling*, 143(1-2):115–146, 2001.

[39] H. O. Pörtner, D. C. Roberts, H. Adams, C. Adler, P. Aldunce, E. Ali, R. A. Begum, R. Betts, R. B. Kerr, R. Biesbroek, et al. Climate change 2022: impacts, adaptation and vulnerability. 2022.

[40] S. Ramondenc, D. Eveillard, L. Guidi, F. Lombard, and B. Delahaye. Probabilistic modeling to estimate jellyfish ecophysiological properties and size distributions. *Scientific reports*, 10(1):1–13, 2020.

[41] C. P. O. Reyer, N. Brouwers, A. Rammig, B. W. Brook, J. Epila, R. F. Grant, M. Holmgren, F. Langerwisch, S. Leuzinger, W. Lucht, B. Medlyn, M. Pfeifer, J. Steinkamp, M. C. Vanderwel, H. Verbeeck, and D. M. Villela. Forest resilience and tipping points at different spatio-temporal scales: Approaches and challenges. *Journal of Ecology*, 103(1):5–15, 2015.

[42] M. Rietkerk, R. Bastiaansen, S. Banerjee, J. van de Koppel, M. Baudena, and A. Doelman. Evasion of tipping in complex systems through spatial pattern formation. *Science*, 374(6564):eabj0359, 2021.

[43] S. Saatchi, M. Longo, L. Xu, Y. Yang, H. Abe, M. Andre, J. E. Aukema, N. Carvalhais, H. Cadillo-Quiroz, G. A. Cerbu, et al. Detecting vulnerability of humid tropical forests to multiple stressors. *One Earth*, 4(7):988–1003, 2021.

[44] C. M. Shackleton. The effects of fire on post-fire seed germination of selected Savanna woody species. *African Journal of Ecology*, 2007.

[45] C. A. d. Silva Junior, M. Lima, P. E. Teodoro, J. F. d. Oliveira-Júnior, F. S. Rossi, B. M. Funatsu, W. Butturi, T. Lourençoni, A. Kraeski, T. D. Pelissari, F. A. Moratelli, D. Arvor, I. M. d. S. Luz, L. P. R. Teodoro, V. Dubreuil, and V. M. Teixeira. Fires Drive Long-Term Environmental Degradation in the Amazon Basin. *Remote Sensing*, 14(2), 2022.

[46] X.-P. Song, M. C. Hansen, S. V. Stehman, P. V. Potapov, A. Tyukavina, E. F. Vermote, and J. R. Townshend. Global land change from 1982 to 2016. *Nature*, 560(7720):639–643, 2018.

[47] A. C. Staver, S. Archibald, and S. A. Levin. The global extent and determinants of savanna and forest as alternative biome states. *science*, 334(6053):230–232, 2011.

[48] T. V. Ta, L. T. H. Nguyen, and A. Yagi. A sustainability condition for stochastic forest model. *Communications on Pure & Applied Analysis*, 16(2), 2017.

[49] S. Tega, V. Yatat, J.-J. Tewa, and P. Couteron. A minimalistic model of spatial structuration of humid savanna vegetation. In *CARI 2020-Colloque Africain sur la recherche en Informatique et en Mathématiques Appliquées*, 2020.

[50] K. Thonicke, M. Bahn, S. Lavorel, R. D. Bardgett, K. Erb, M. Giamberini, M. Reichstein, B. Vollan, and A. Rammig. Advancing the understanding of adaptive capacity of social-ecological systems to absorb climate extremes. *Earth's Future*, 8(2):e2019EF001221, 2020.

[51] N. Timilsina, F. J. Escobedo, C. L. Staudhammer, and T. Brandeis. Analyzing the causal factors of carbon stores in a subtropical urban forest. *Ecological Complexity*, 20:23–32, 2014.

[52] J. Towner, H. L. Cloke, W. Lavado, W. Santini, J. Bazo, E. C. de Perez, and E. M. Stephens. Attribution of Amazon floods to modes of climate variability: A review. *Meteorol. Appl.*, 27:e1949, 2020.

[53] H. L. Younes and R. G. Simmons. Probabilistic verification of discrete event systems using acceptance sampling. In *International Conference on Computer Aided Verification*, pages 223–235. Springer, 2002.

[54] P. Zelazowski, Y. Malhi, C. Huntingford, S. Sitch, and J. B. Fisher. Changes in the potential distribution of humid tropical forests on a warmer planet. *Philosophical Transactions of the Royal Society A: Mathematical, Physical and Engineering Sciences*, 369(1934):137–160, 2011.